Manuscript Details

Manuscript number	JCOU_2019_51
Title	Pt nanoparticles-loaded and noble-metal-free, mesoporous oxides as efficient catalysts for CO2 hydrogenation and dry reforming with methane
Short title	Noble-metal-free, mesoporous oxides for CO2 activation reactions
Article type	Full Length Article

Abstract

In this study, a series of free-standing as well as controlled size Pt nanoparticles-loaded mesoporous metal oxides (CeO2, MnO2, In2O3, NiO, and Co3O4) with high surface area and designed pore structure were prepared by hard template method and used as catalysts for CO2 hydrogenation as well as dry reforming of CO2 with methane. The physicochemical properties of catalysts were characterized by N2 adsorption-desorption isotherm, XRD, TEM, and H2-TPR. Pt-free and Pt-loaded mesoporous NiO and Co3O4 performed with high catalytic activity and selectivity for both CO2 activation reactions. Pt-free NiO exhibited the highest catalytic activity as well as showing 100 % CH4 selectivity at 473 - 673 K and ~1:1 H2/CO2 ratio at 673 – 973 K in CO2 hydrogenation and dry reforming with methane, respectively. The enhanced catalytic properties can be ascribed to the presence of metallic Ni as well as the optimal dynamics of Ni/NiOx structure under reaction conditions.

Keywords	Mesoporous oxides, Pt nanoparticles, CO2 hydrogenation, dry reforming of CO2

Corresponding Author	András Sápi
Order of Authors	András Sápi, Rajkumar Thangavel, Marietta Ábel, Anastasiia Efremova, András Grósz, Anett Gyuris, Kornélia B. Ábrahámné, Imre Szenti, Janos Kiss, Tamás Varga, Akos Kukovecz, Zoltan KONYA

Suggested reviewers	Hailiang Wang, Kim Chang Min, Gabor Somorjai, Robert Vajtai

Submission Files Included in this PDF

File Name [File Type]

Cover letter.doc [Cover Letter]

Paper final (1).docx [Manuscript File]

To view all the submission files, including those not included in the PDF, click on the manuscript title on your EVISE Homepage, then click 'Download zip file'.

Research Data Related to this Submission

There are no linked research data sets for this submission. The following reason is given:
Data will be made available on request

UNIVERSITAS SCIENTIARUM SZEGEDIENSIS
SZEGEDI TUDOMÁNYEGYETEM

Dear Sang-Eon Park (Editor-in-Chief, Journal of CO_2 Utilization),

Please find our manuscript *"Pt nanoparticles-loaded and noble-metal-free, mesoporous oxides as efficient catalysts for CO_2 hydrogenation and dry reforming with methane"* submitted to Journal of CO2 utilization.

In this paper, we tested several Pt-free as well as controlled sized Pt nanoparticle-loaded mesoporous transient metal oxides with high surface area in CO_2 hydrogenation as well as CO_2 dry reforming with methane. Pt-free and Pt-loaded mesoporous NiO and Co_3O_4 performed with high catalytic activity and selectivity for both CO_2 activation reactions. Pt-free NiO exhibited the highest catalytic activity as well as showing 100 % CH_4 selectivity at 473 - 673 K and ~1:1 H_2/CO_2 ratio at 673 – 973 K in CO_2 hydrogenation and dry reforming with methane, respectively. The enhanced catalytic properties can be ascribed to the presence of metallic Ni as well as the optimal dynamics of Ni/NiO_x structure under reaction conditions.

Also, we confirm that this manuscript has not been published elsewhere and is not under consideration by another journal. All authors have approved the manuscript and agree with its submission to *Journal of CO_2 utilization*.

We suggest the following objective reviewers for the manuscript:

1. Prof. Gabor A. Somorjai, University Professor, College of Chemistry, UC Berkeley, CA, USA
   somorjai@berkeley.edu, http://www.cchem.berkeley.edu/gasgrp/

2. Dr. Hailiang Wang, Assistant Professor of Chemistry, Department of Chemistry, Yale University, CT, USA
   hailiang.wang@yale.edu, http://wanglab.yale.edu/

3. Dr. Selim Alayoglu, CSD Project Scientist, Lawrence Berkeley National Laboratories, Berkeley, CA, USA
   SAlayoglu@lbl.gov, https://commons.lbl.gov/display/csd/Selim+Alayoglu

4. Prof. Wei-Fang Su, Professor, Department of Materials Science and Engineering, National Taiwan University, Taiwan

András SÁPI, PhD.
Dept. of Applied & Environmental Chemistry
University of Szeged, 1. Rerrich Square, H-6720 Szeged
Tel: 62/343-795, Fax: 62/544-619
WEB: http://www.staff.u-szeged.hu/~sapia/ E-mail: sapia@chem.u-szeged.hu

suwf@ntu.edu.tw, http://www.mse.ntu.edu.tw/~frontier/profileE1.htm

5. Dr. Robert Vajtai, Senior Faculty Fellow, Department of Materials Science and NanoEngineering (MSNE), Rice University, TX, USA
   vajtai@rice.edu, http://msne.rice.edu/Content.aspx?id=108

6. Dr. Geza Toth, Faculty Member, Faculty of Information Technology and Electrical Engineering, University of Oulu. Finland
   geza@ee.oulu.fi, http://www.oulu.fi/eeng/personnel/toth-geza

7. Prof. Kim Chang Min, Professor, College of Natural Sciences, Kyungpook National University, Daegu, South Korea

   cmk@knu.ac.kr

Your Faithfully,

18th of January, 2019. Dr. András Sápi

Pt nanoparticles-loaded and noble-metal-free, mesoporous oxides as efficient catalysts for CO_2 hydrogenation and dry reforming with methane

András Sápi[*,Φ,†], *T. Rajkumar*[†], *Marietta Ábel*[†], *Anastasiia Efremova*[†], *András Grósz*[†], *Anett Gyuris*[†], *Kornélia B. Ábrahámné*[†], *Imre Szenti*[†], *János Kiss*[Ψ,†], *Tamás Varga*[†], *Ákos Kukovecz*[†], *Zoltán Kónya*[†,Ψ]

[†] Department of Applied and Environmental Chemistry, University of Szeged, H-6720 Szeged, Hungary

[Φ] Institute of Environmental and Technological Sciences, University of Szeged, H-6720 Szeged, Hungary

[Ψ] MTA-SZTE Reaction Kinetics and Surface Chemistry Research Group, University of Szeged, H-6720 Szeged, Hungary

Abstract

In this study, a series of free-standing as well as controlled size Pt nanoparticles-loaded mesoporous metal oxides (CeO_2, MnO_2, In_2O_3, NiO, and Co_3O_4) with high surface area and designed pore structure were prepared by hard template method and used as catalysts for CO_2 hydrogenation as well as dry reforming of CO_2 with methane. The physicochemical properties of catalysts were characterized by N_2 adsorption-desorption isotherm, XRD, TEM, and H_2-TPR. Pt-free and Pt-loaded mesoporous NiO and Co_3O_4 performed with high catalytic activity and selectivity for both CO_2 activation reactions. Pt-free NiO exhibited the highest catalytic activity as well as showing 100 % CH_4 selectivity at 473 - 673 K and ~1:1 H_2/CO_2 ratio at 673 – 973 K in CO_2 hydrogenation and dry reforming with methane, respectively. The enhanced catalytic properties can be ascribed to the presence of metallic Ni as well as the optimal dynamics of Ni/NiO_x structure under reaction conditions.

Key words: *Mesoporous oxides, Pt nanoparticles, CO_2 hydrogenation, dry reforming of CO_2*

1. Introduction

Recently, the population increase and connecting industrial demands has caused a tremendous amount of fossil fuel utilization. The combustion of fossil fuels leads to the release of CO_2 into the atmosphere which in turn leads to global warming and climate change [1].

The hydrogenation of CO_2 leads to the formation of a variety of products e.g., methanol (CH_3OH), carbon monoxide (CO), methane (CH_4), formic acid (HCOOH) and hydrocarbons [2-7]. CO_2 hydrogenation through the reverse water-gas shift reaction produces the primary industrial C_1 building block CO which, together with H_2, can be used to produce long-chain hydrocarbons through Fischer-Tropsch reaction [8, 9].

$$CO_2 + H_2 \longrightarrow CO + H_2O \quad \Delta H = 42.2 \text{ kJ mol}^{-1}$$

However, CO_2 hydrogenation is an endothermic reaction and requires high operation temperature [10]. Various metals such as Pt [11-14], Pd [15-18], Rh [19-24] and Au [25, 26], Ru [27], Cu [28-30], Fe [31, 32], and Ni [33, 34] have been utilized. Various supports such as CeO_2 [28, 35, 36], SiO_2 [37, 38], Al_2O_3 [39, 40], ZrO_2 [29], TiO_2 [25, 41], zeolite [13] have been used. In addition, methanation of CO_2, also known as Sabatier reaction is a promising strategy for the production of methane. It is an exothermic reaction and favors formation of methane at high pressure and low temperature.

$$CO_2 + 4H_2 \longrightarrow CH_4 + 2H_2O \quad \Delta H = -165 \text{ kJ mol}^{-1}$$

This reaction is the key to the Power-to-gas (PtG) technology. PtG is the production of chemical energy carriers using electric power during peak power production period. PtG involves two steps. The first step is to produce hydrogen by water electrolysis. The second step is the methanation (Sabatier reaction) between H_2 and CO_2 to produce synthetic natural gas (SNG) [42, 43]. The produced SNG is easy to store and can be transported in existing natural gas pipelines. A variety of transition metals such as Ni [44-46], Co [47-49], Pd [50, 51], Ru [52-54], Rh [55, 56] have been widely investigated as active components for CO_2 methanation. Among these metals, Ni and Co are promising candidates due to its lower cost than Pd, Ru, and Rh. A variety of oxide supports have been used for the CO_2 methanation that includes Al_2O_3 [57-59], SiO_2 [47, 60, 61], TiO_2 [52, 53, 62, 63], CeO_2 [50, 61, 64], NiO [65], Co_3O_4 [66]. Supported noble metal catalysts such as Pt, Ru, and Rh was found to have high ability toward H_2 dissociation and thus have been used as effective catalysts for CO_2 hydrogenation [2]. The

activity and selectivity of supported catalysts are associated with interactions between the active metals and oxide supports [3]. The ordered mesoporous metal oxides and SBA-15 with tunable pore size and a high specific surface area have provided an opportunity not only for the high conversion but also for the synthesis of well-dispersed metal catalysts.

In the dry reforming of methane (DRM) reaction, two major greenhouse gases (CH_4 and CO_2) are converted into syngas (H_2 and CO). The formed syngas can be used in Fischer-Tropsch reaction [67].

$$CH_4 + CO_2 \longrightarrow 2CO + 2H_2 \quad \Delta H = 247 \text{ kJ mol}^{-1}$$

DRM is a highly endothermic reaction and therefore high temperatures are needed to obtain high syngas yields [68]. DRM reaction has been carried out by using various heterogeneous catalysts. The noble metals such as Rh, Ir, Pt, Ru, and Pd exhibit higher catalytic activity and stability compared to other transition metal-based catalysts (Ni and Co) [69-74]. Ni-based catalysts are extensively used due to their high catalytic activity and low cost. However, due to coke formation and sintering during the long-term run, their activity was found to be poor [75]. Extensive research has been done on designing coke-resistant catalysts for DRM. Various transition metal oxide [76, 77], post-transition metal oxides [78], and rare earth metal oxide [79-81], SBA-15 [82] have been used as a catalyst.

In this study, we synthesized mesoporous metal oxides such as CeO_2, MnO_2, In_2O_3, NiO, Co_3O_4, and SBA-15 with high specific surface and anchored size controlled Pt nanoparticles on these oxides. The synthesized catalysts were characterized by N_2 adsorption-desorption isotherm, XRD and TEM. CO_2 hydrogenation and DRM reactions were carried out on these catalysts to evaluate their catalytic efficiencies. NiO and Co_3O_4 based catalysts showed significant activity in both CO_2 activation reactions. Due to the reduction of the oxides, a special Ni/NiO_x as well as a Co/CoO_x interphase is produced during the reactions which may be attributed to the high activity even in the absence of Pt nanoparticles. In the case of pure NiO support, the activity was observed as ~2 times and ~3 times higher compared to the Pt/NiO catalysts at the hydrogenation reaction at ~600 K and the DRM reaction at ~900 K, respectively.

2. Experimental

2.1 Synthesis of catalysts

2.1.1 Synthesis of 4.8 nm Pt nanoparticles

Synthesis of 4.8 nm particles is based on a modified version of the polyol-method. Briefly, 0.04 g $Pt(C_5H_7O_2)_2$ and 0.035 g polyvinylpyrrolidone (PVP, MW = 40,000) are dissolved in 5 ml ethylene-glycol and ultrasonicated for 30 minutes to get a homogenous solution. The reactor is a three-necked round bottom flask, which is evacuated and purged with atmospheric pressure argon gas for several cycles to get rid of additional oxygen and water. After three purging cycles, the flask was immersed in an oil bath heated to 473 K under vigorous stirring of the reaction mixture as well as the oil bath. After 10 minutes of reaction, the flask was cooled down to room temperature. The suspension is precipitated with adding acetone and centrifuging. The nanoparticles are washed by centrifuging with hexane and redispersing in ethanol for at least 2-3 cycles and finally redispersed in ethanol.

2.1.2 Synthesis of the mesoporous metal oxide support

For the preparation of mesoporous metal-oxide support, mesoporous KIT-6 silica was used as hard template [83]. For the synthesis of KIT-6, 27 g of the Pluronic-123 block copolymer and 43.5 ml HCl was dissolved in 980 ml water. After 30 min, 33.3 ml n-butanol was added to the solution at 35 °C under vigorous stirring. After 1 h of stirring, 58 g of Tetraethyl orthosilicate (TEOS) was added to the solution dropwise followed by stirring for 24 h at 308 K. The capped bottle was stored at 313 K for another 24 h in an oven. Then the solid product was filtered, dried at 363 K overnight and calcined at 823 K for 6 h.

Mesoporous oxides were prepared through the hard template method using the as-prepared KIT-6. $Ce(NO_3)_3.6H_2O$, $Mn(NO_3)_2.xH_2O$, $In(NO_3)_3.xH_2O$, $Ni(NO_3)_2.6H_2O$ and $Co(NO_3)_2.6H_2O$ were used to synthesis mesoporous CeO_2, MnO_2, In_2O_3, NiO and Co_3O_4 respectively. In a typical synthesis, 16 mmol of metal nitrate was dissolved in 8 ml water and mixed with a suspension of 4 g KIT-6 in 50 ml toluene. The mixture was stirred at 338 K to completely evaporate toluene. After the evaporation, the precipitated product was collected and dried at 333 K overnight, followed by calcination at 573 K for 6 h. The silica template was completely removed by several washing steps using 2 M aqueous NaOH solution. The filtered product was dried at 323 K.

2.1.3 Synthesis of the SBA-15 mesoporous silica support

SBA-15 mesoporous silica support was synthesized from tetraethyl orthosilicate (TEOS) by a soft template method. 8 g of pre-melted Pluronic-123, 60 ml of distilled water and 240 ml of 2 M HCl solution were mixed together at 313 K for 2 hours. After the dissolution of P-123, 17 g of TEOS was added dropwise to the mixture at 313 K and continuous stirring was applied for 20 hours. Stirring was continued for 1.5 days at 333 K. After the synthesis, the product was filtered and washed with distilled water. Then, the product was heated to 373 K with a heating rate of 2 K min^{-1} and aged for 5 hours, then the temperature was increased to 823 K with a heating rate of 1 K min^{-1}. After 4 hours of calcination, the product is ready for further use.

2.1.4 Synthesis of Mesoporous metal oxide and SBA-15 supported Pt catalysts

To fabricate supported catalysts, the ethanol suspension of Pt nanoparticles to reach a loading of 0.5 wt % and the different supports were mixed together in ethanol and sonicated in an ultrasonic bath (40 kHz, 80 W) for 3 hours. The supported nanoparticles were collected by centrifugation. The products were washed with ethanol three times before they were dried at 353 K overnight. The required amount of Pt nanoparticle suspension was calculated based on ICP measurements.

2. 2 Characterization of catalysts

2.2.1 Transmission Electron Microscopy (TEM)

Imaging of the all the samples were carried out using an FEI TECNAI G2 20 X-Twin high-resolution transmission electron microscope (equipped with electron diffraction) operating at an accelerating voltage of 200 kV. The samples were drop-cast onto carbon film coated copper grids from ethanol suspension.

2.2.2 Powder X-ray Diffraction (XRD)

XRD studies of all samples were performed on a Rigaku MiniFlex II instrument with a Ni-filtered CuKα source in the range of 2θ = 10-80°.

2.2.3 N_2 adsorption-desorption isotherm measurements

The specific surface area (BET method), the pore size distribution and the total pore volume were determined by the BJH method using a Quantachrome NOVA 2200 gas sorption

analyzer by N_2 gas adsorption/desorption at 77 K. Before the measurements, the samples were pre-treated in a vacuum (<~0.1 mbar) at 473 K for 2 hours.

2.2.4 Temperature Programmed Reduction (TPR)

The temperature-programmed reduction (TPR) was carried out in a BELCAT-A apparatus using a reactor (quartz tube with 9 mm outer diameter) that was externally heated. Before the measurements, the catalyst samples were treated in oxygen at 673 K for 30 min. Thereafter, the sample was cooled in flowing Ar to room temperature. The oxidized sample was flushed with N_2 containing 10% H_2, the reactor was heated linearly at a rate of 5 K/min from 323 K to 773 K and the H_2 consumption was detected by a thermal conductivity detector (TCD).

2.2.5 Hydrogenation of carbon-dioxide in a continuous flow reactor

Before the catalytic experiments, the as-received catalysts were oxidized in O_2 atmosphere at 573 K for 30 min to remove the surface contaminants as well as the PVP capping agent and thereafter were reduced in H_2 at 573 K for 60 min.

Catalytic reactions were carried out at atmospheric pressure in a fixed-bed continuous-flow reactor (200 mm long with 8 mm i.d.), which was heated externally. The dead volume of the reactor was filled with quartz beads. The operating temperature was controlled by a thermocouple placed inside the oven close to the reactor wall, to assure precise temperature measurement. For catalytic studies, small fragments (about 1 mm) of slightly compressed pellets were used. Typically, the reactor filling contained 150 mg of catalyst. In the reacting gas mixture, the CO_2: H_2 molar ratio was 1:4, if not denoted otherwise. The CO_2: H_2 mixture was fed with the help of mass flow controllers (Aalborg), the total flow rate was 50 ml/min. The reacting gas mixture flow entered and left the reactor through an externally heated tube in order to avoid condensation. The analysis of the products and reactants was performed with an Agilent 6890 N gas chromatograph using HP-PLOTQ column. The gases were detected simultaneously by thermal conductivity (TC) and flame ionization (FI) detectors. The CO_2 was transformed by a methanizer to methane and it was also analysed by FID.

2.2.6 Dry reforming of methane in a continuous flow reactor

We used the same reaction conditions as that used for CO_2 hydrogenation reaction except that the CH_4: CO_2 ratio was maintained at 1:1 with the total flow rate of 60ml/min.

3. Results and Discussion

3.1 N_2 adsorption-desorption analysis

The N_2 adsorption-desorption isotherms of the catalysts are shown in Fig. 1. All catalysts exhibit a high surface area (80 – 133 m^2g^{-1} for transition metal oxides and 786 m^2g^{-1} for SBA-15 oxide), as well as type IV adsorption isotherms with hysteresis loop at the high relative pressure region, which is a distinctive feature of capillary condensation in mesopores [84]. The specific surface area, pore diameter and pore volume of all catalysts are presented in Table 1. CeO_2 presented a specific surface area of 133 m^2g^{-1} and pore volume of 0.2134 cm^3g^{-1} which is very high compared to those obtained by conventional precipitation method [85]. MnO_2 exhibits hysteresis loop in the relative pressure range 0.3 to 1 with type IV isotherm and H3 type hysteresis indicates the presence of mesopores in the sample [86].

In_2O_3 exhibits type IV adsorption isotherm according to IUPAC classification [87]. Co_3O_4 with a specific surface area of 94.691 m^2g^{-1} and pore volume of 0.1218 cm^3g^{-1} exhibits H3 type hysteresis loops indicating the presence of slit-shaped pores [88]. NiO displayed a specific surface area of 107.059 m^2g^{-1} and pore volume of 0.1922 cm^3g^{-1}. NiO exposes a type IV adsorption isotherm with an H3 type hysteresis loop in the relative pressure range of 0.3-1.0 [89]. SBA-15 exhibited high BET surface area of 786.3 m^2g^{-1} and pore volume of 0.7002 cm^3g^{-1} which is comparable with other studies [90]. SBA-15 displayed type IV adsorption isotherm with an H1 type hysteresis loop in the relative pressure range of 0.5-0.7 which is indicative of narrow pore size distribution according to IUPAC classification [91].

Table 1. *Adsorption properties (specific surface area, pore diameter and pore volume) of the catalysts*

Sample	**BET surface area (m^2g^{-1})**	**Pore diameter (nm)**	**Pore volume ($cm^3\ g^{-1}$)**
CeO_2	133.231	3.58	0.2134
Co_3O_4	94.691	3.58	0.1218
In_2O_3	88.000	3.80	0.1240
MnO_2	136.973	3.60	0.2141
NiO	107.059	3.86	0.1922
SBA-15	786.370	4.00	0.7002

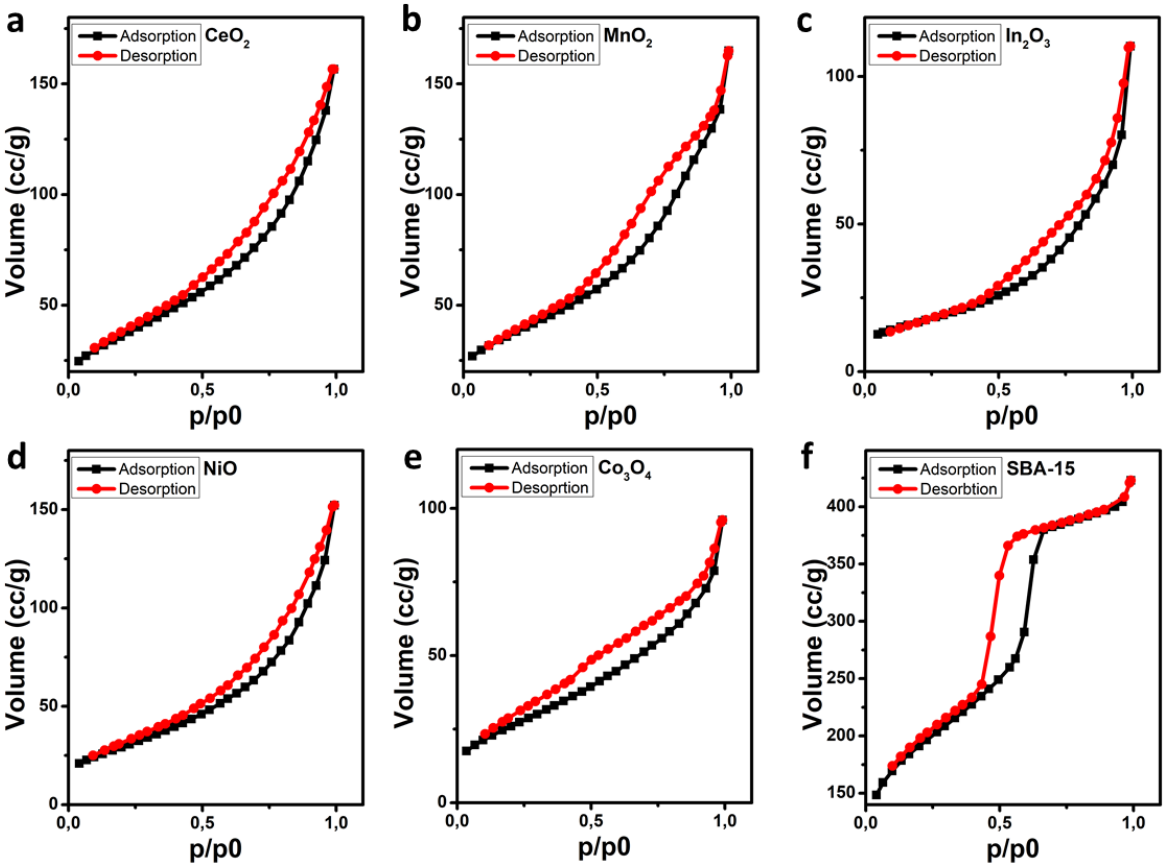

Fig. 1. *N_2 adsorption desorption isotherm of (a) CeO_2 (b) MnO_2 (c) In_2O_3 (d) NiO(e) Co_3O_4 (f) SBA-15*

3.2 X-ray Diffraction

The XRD patterns of mesoporous CeO_2, MnO_2, In_2O_3, NiO, and Co_3O_4 shows the presence of low intensity and elongated peaks characteristic for nanostructured materials with low crystallinity (Fig. 2). Fig. 2(a) shows the XRD pattern of CeO_2. The peaks at 28.6°, 33.1°, 47.6°, 56.3°, 59.3°, 69.3° and 76.8° were corresponded to the (111), (200), (220), (311), (222), (400) and (331) planes (JCPDS No. 34-0394), respectively of the face-centered cubic structure of CeO_2 (a = 5.411 Å, space group: fm3m) [92]. XRD pattern of MnO_2 is shown in Fig. 2(b). Diffraction peaks at 28.8°, 37.2°, 42.7° and 56.5° corresponds to crystal planes of (110), (101), (111) and (211), respectively (JCPDS No. 44-0141) [93]. It can be indexed to the tetragonal crystal structure of α-MnO_2. The diffraction pattern clearly corroborates the phase purity of the prepared α-MnO_2. XRD pattern of In_2O_3 is shown in Fig. 2(c). The diffraction peaks at 21.4°, 30.6°, 35.4°, 51°, 60.6° corresponds to crystal planes of (211), (222), (400), (440), and (622) respectively for In_2O_3 cubic structure [94].

XRD pattern of NiO is shown in Fig. 2 (d). The diffraction peaks at 37.2°, 43.2°, 62.8°, 75.2° and 79.3° were indexed to (111), (200), (220), (311) and (222) planes respectively. It can be indexed to the face-centered cubic NiO phase (Fm-3m, JCPDS No. 47-1049) [95]. Fig. 2(e) shows the XRD pattern of Co_3O_4. The peaks at 19°, 31.3°, 36.7°, 38.6°, 44.8°, 55.3°, 59.2° and 65.35° corresponds to crystal planes of (111), (220), (311), (222), (400), (422), (511) and (440) respectively for Co_3O_4 cubic spinel structure (JCPDS card No.43-1003) [96].

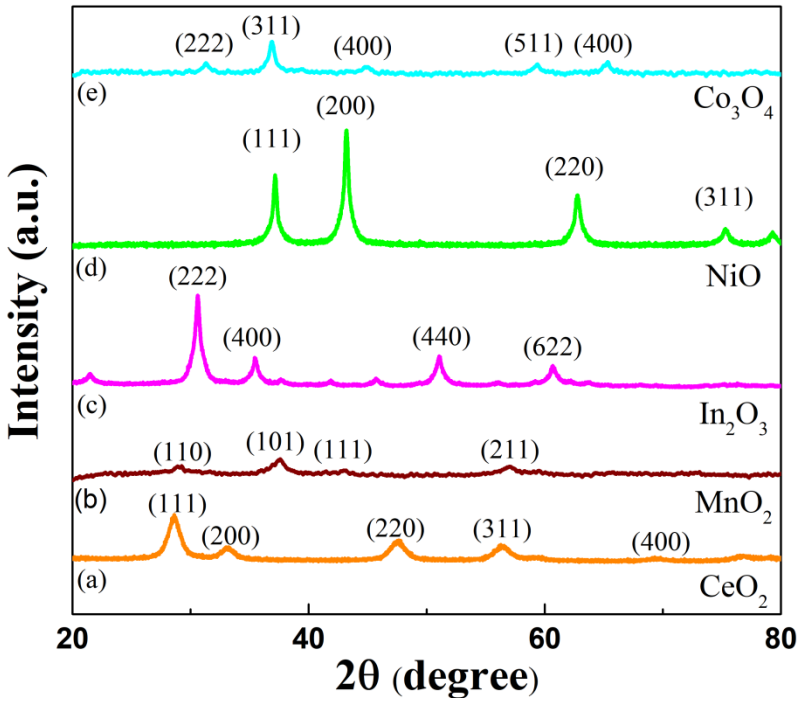

Fig. 2. *XRD patterns of (a) CeO_2 (b) MnO_2 (c) In_2O_3 d) NiO (e) Co_3O_4*

3.3 Transmission Electron Microscopy

The morphology of as-synthesised samples was examined by Transmission Electron Microscopy (TEM). Fig. 3 shows the TEM images of the mesoporous oxides. The ordered pore structure is presented for all oxides, where the average pore size is 2-5 nm and the wall thickness is ~ 5-7 nm. The length of the pore structure can be varied from 100 nm to a several hundreds of nanometer. Fig. 3(f) shows the TEM image of the SBA-15. The image clearly shows well-ordered mesoporous hexagonal arrays.

TEM images of the 0.5 % Pt nanoparticles anchored onto the surface of the mesoporous CeO_2, MnO_2, NiO, Co_3O_4 and SBA-15 are shown in Fig. 4. The surface dispersion of the Pt nanoparticles is homogeneous without presence of aggregated Pt nanoparticles. The size of the

Pt nanoparticles was 4.8 ± 1.2 nm with narrow size distribution while the shape of the particles was mostly polyhedral with multiple facets close to a spherical structure.

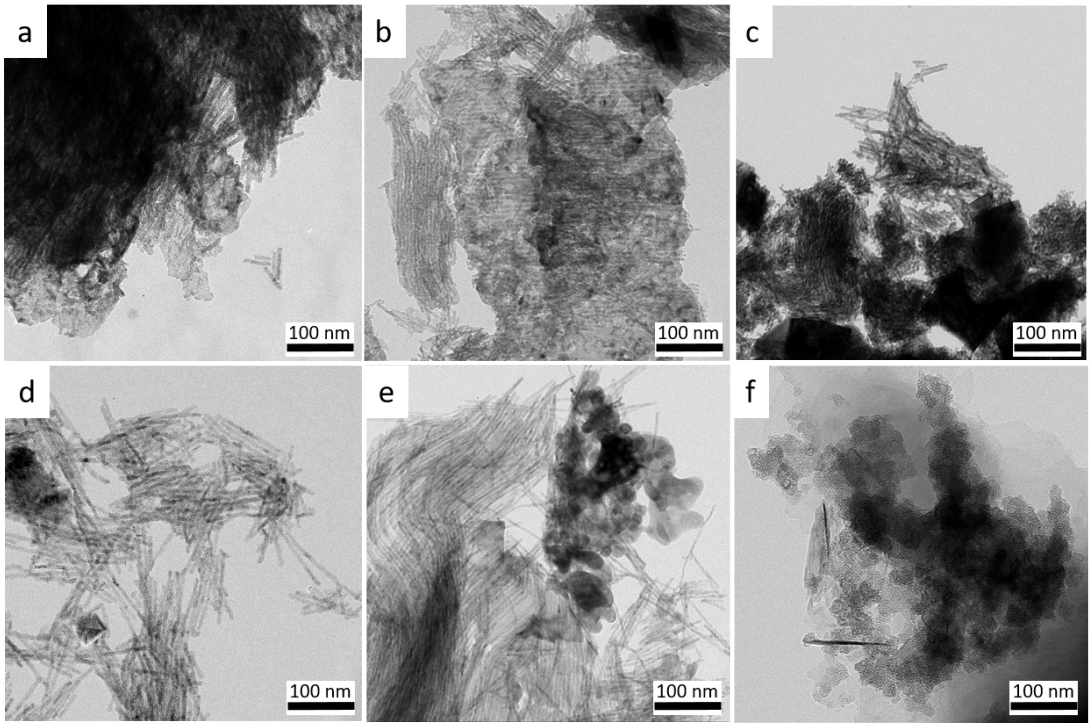

Fig. 3. *TEM images of free-standing mesoporous (a) CeO_2 (b) MnO_2 (c) In_2O_3 (d) NiO (e) Co_3O_4 and (f) SBA-15*

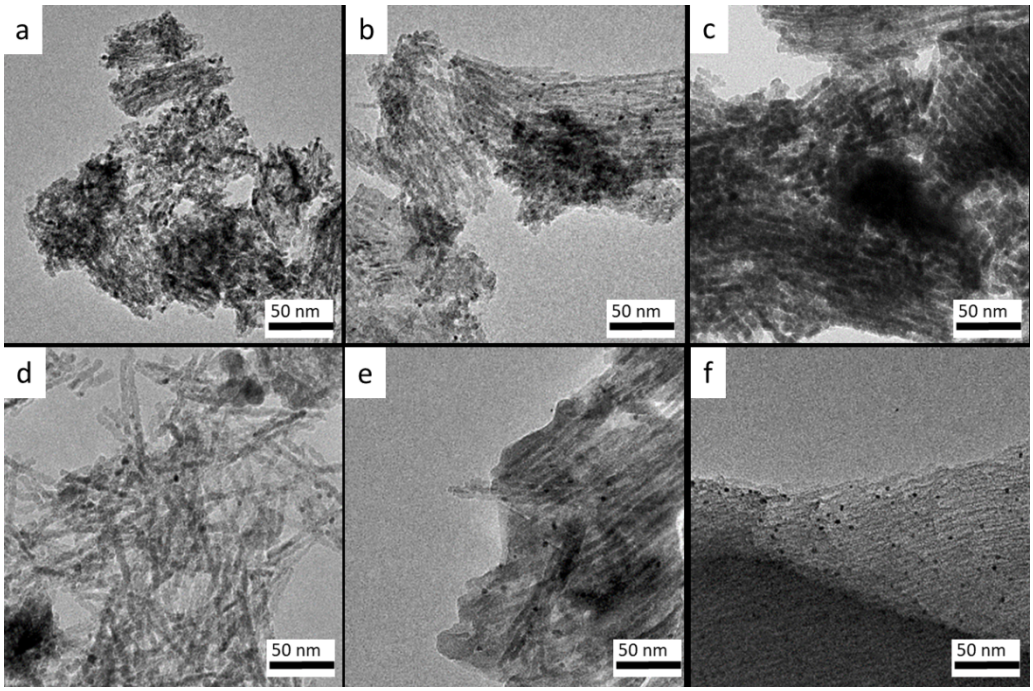

Fig. 4. *TEM images of (a) 0.5 % Pt/CeO_2 (b) 0.5 % Pt/MnO_2 (c) 0.5 % Pt/In_2O_3 (d) 0.5 % Pt/NiO (e) 0.5 % Pt/Co_3O_4 (f) 0.5 % Pt/SBA-15*

3.4 Temperature-Programmed Reduction

The reducibility properties of catalysts were tested by Temperature Programmed Reduction by Hydrogen gas (H_2-TPR) and the results are presented in Fig. 5. The total H_2 consumed and the reduction temperatures during the H_2-TPR is presented in Table 2. The reducibility of the mesoporous metal oxides differ from most oxide type used in the literature. The differences can be interpreted due to the structural differences. For CeO_2 and Pt/CeO_2, no characteristic reduction peak was observed in our studied temperature region of 323-773 K, only a small reduction peak can be detected at around 391 K which may be identified as a partial reduction of surface layer. However, pure CeO_2 reduction are observed with two peaks in the TPR as reported in the literature [97, 98]. The first peak at ~532 K can be attributed to the reduction of surface oxygen species and the second peak at ~670 K can be attributed to the reduction of bulk lattice oxygen of CeO_2. When Pt nanoparticles are also presented on the surface of the supports, an additional small peak appeared at 391 K showing the presence of the metal oxide reducing effect of the Pt nanoparticles.

MnO_2 shows two reduction peaks at 540 and 630 K with a total H_2 consumption of 7.2 mmol/g (Table 2). The lower temperature reduction peak can be attributed to the reduction of MnO_2 to Mn_3O_4 and the peak at the higher temperature is due to the reduction of Mn_3O_4 to MnO [99]. In the case of the Pt/MnO_2 catalysts, however, one intense reduction peak at 440 K with 5.7 mmol/g H_2 consumption was observed showing that a large part of MnO_2 reduced at a lower temperature due to SMSI between Pt and MnO_2. This is also in consistent to the reduced intensity of the peak at 530 K. The shift towards lower temperature for MnO_2 after Pt loading can be attributed to activation of H_2 on the pre-reduced Pt and the spillover of this activated hydrogen on MnO_2 which largely promoted the reduction of MnO_2 [100, 101].

For In_2O_3 and Pt/In_2O_3 (not shown), no characteristic reduction peak was observed in our studied temperature region of 323-773 K. However, pure In_2O_3 reduces to metallic indium around 973 K as reported in the literature [102].

NiO shows a reduction peak at 650-767 K which can be attributed to the reduction of NiO to metallic nickel [69, 103, 104]. Pt/NiO show the red shift of the reduction temperature of the nickel oxide reduction showing the presence of the promoting effect of Pt on the reduction of NiO and the reduction of NiO_x species [69].

The TPR profile of Co_3O_4 shows two peaks. The low-temperature peak at 563 K can be attributed to the reduction of surface Co^{3+} to Co^{2+} and the high-temperature peak at 667 K is due to the reduction of Co^{2+} to metallic cobalt [69, 98, 105]. For Pt/Co_3O_4 catalysts, all the reduction peaks are shifted to lower temperatures and the catalyst showed a low temperature peak at 387 K and a high-temperature peak at 533 and 606 K. The decrease of reduction temperature for Pt/Co_3O_4 compared to Co_3O_4 can be attributed to the spillover of H_2 from Pt to Co_3O_4 [106] as well as the oxygen removing behavior of Pt from the oxide structure [65].

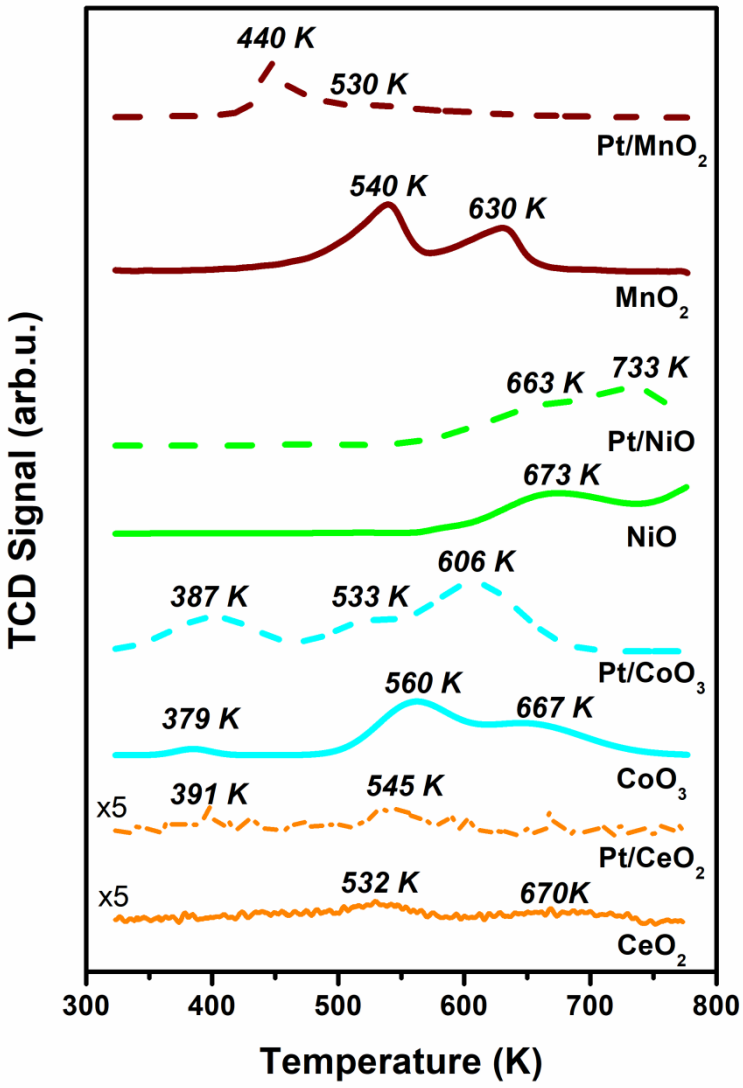

Fig.5 *H_2-TPR profiles CeO_2 and 0.5 % Pt/CeO_2, Co_3O_4 and 0.5 % Pt/Co_3O_4, NiO and 0.5 % Pt/NiO, MnO_2 and 0.5 % Pt/MnO_2*

Table 2. *H_2 temperature-programmed reduction data for the catalysts*

Catalysts	H_2-TPR	
	Peak positions (K)	**H_2 consumption (mmol g^{-1})**
MnO_2	540. 630	7.2
Pt/MnO_2	633 (shoulder)	5.7
NiO	535. 667	7.2
Pt/NiO	633	8.7
Co_3O_4	560. 667	8.3
Pt/Co_3O_4	119. 338	11.6
CeO_2	527	0.5
Pt/CeO_2	391. 545	0.5

3.5 Catalytic activity tests

3.5.1 CO_2 hydrogenation reaction

The catalytic efficiencies of CeO_2, MnO_2, In_2O_3, NiO, and Co_3O_4 for CO_2 hydrogenation is shown in Fig. 6 (a), Fig. 7 (a) and Table 3. The major products obtained were CO and CH_4 besides water. The catalytic activity for CO_2 hydrogenation was tested in the temperature range of 475 -675 K. The conversion of CO_2 was increased with the increasing reaction temperature with significant conversion started only at a temperature above 523 K. The conversion reached 80.6% over NiO and 58.4% over Co_3O_4 at 638 K. The high conversion over NiO and Co_3O_4 can be attributed to the presence of Ni/NiO_x and Co/CoO_x structure under reaction conditions [65]. However, further increasing temperature leads to a decrease in conversion presumably due to coke formation on the surface of the catalyst as well as the over-reduction of the oxide resulted in a non-optimal metal/metal-oxide interphase. The other catalysts such as CeO_2, MnO_2, and In_2O_3 do not show any significant conversion. The inactivity can be attributed to the difficulty of the reduction of such metals from their oxides as well as the sintering of these metal oxides under reaction conditions as indicated by X-ray diffraction (Fig. 12.).

The effect of the loading of the 4.8 nm Pt nanoparticles on the catalytic performances of CeO_2, MnO_2, In_2O_3, NiO, Co_3O_4, and SBA-15 was also investigated in the range of 473-673

K (Fig. 6 (b) and Fig. 7 (b)). In the case of the Pt/NiO catalysts, loading of Pt nanoparticles show no significant promotion of the activity of the catalysts. This interesting phenomena is not unusual. In an earlier study we found that Pt has a small effect of Pt/NiO activity compared to the pure NiO support where the 70 % of the surface of the nickel-oxide support was in a metallic state under reaction condition which was promoted by the reduction by the Pt nanoparticles [65]. In this study, the 0.5 % Pt nanoparticle concentration of the catalysts resulted in a surface mixture of $Pt/PtO_x/Ni/NiO_x$ which is not as effective in catalysis as the pure Ni/NiO_x evolved at the surface of the Pt-free mesoporous nickel-oxide under the conditions of CO_2 hydrogenation.

The catalytic activity of Pt/Co_3O_4 catalysts was ~1.5 times higher compared to the pure Co_3O_4 catalysts at 623 K. Ouyang et al prepared Pt/Co_3O_4 and found that the presence of metallic Co after reduction at 473 K had strong hydrogenation ability which in turn leads to higher CO_2 conversion [106]. Here, the formation of the mixed cobalt-oxide structure with the metallic cobalt and Pt on the surface are resulted in a higher activity.

Conversion profile for Pt/CeO_2 and Pt/In_2O_3 are almost identical to the Pt-free catalysts. However, in the case of Pt/MnO_2, the conversion values can be observed as ~ 20 % at 623 K, which is ~ 20 times more compared to the catalytic activity of pure MnO_2.

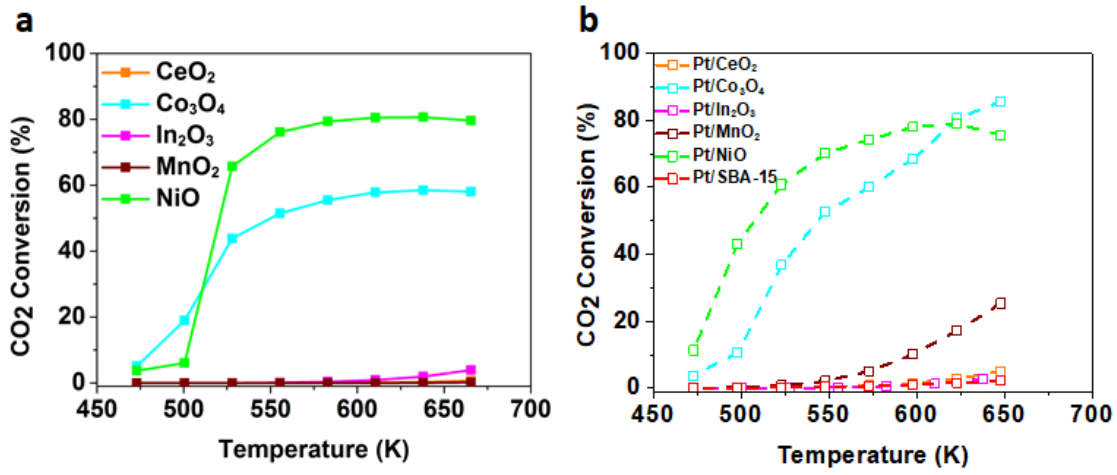

Fig. 6. *Conversion of CO_2 as a function of temperature in the CO_2 hydrogenation reaction over (a) Pt-free mesoporous oxides and (b) Pt-loaded mesoporous oxides*

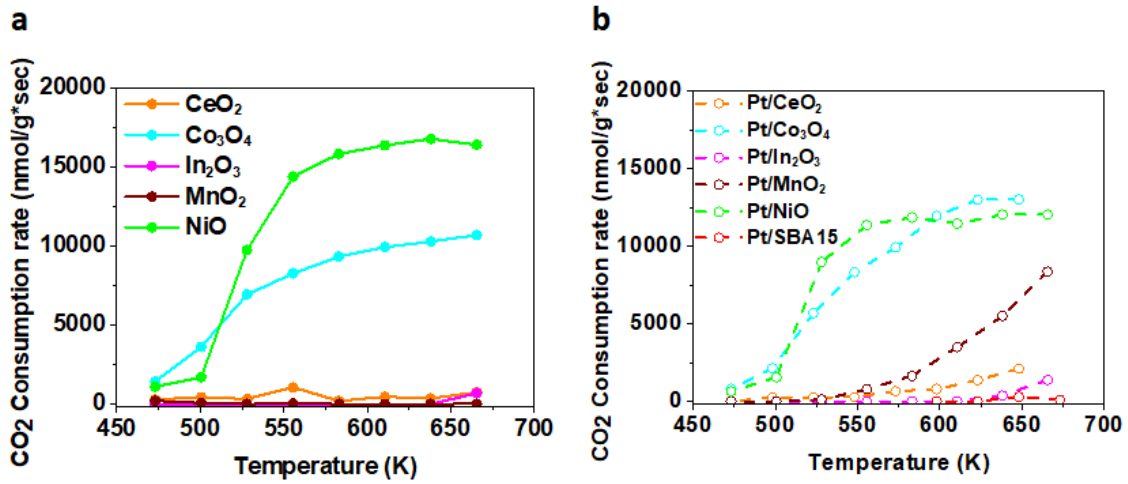

Fig. 7. *CO_2 consumption rate as a function of temperature over (a) pure mesoporous oxides and (b) Pt-loaded mesoporous oxide catalysts in CO_2 hydrogenation reaction*

Table 3. *The highest CO_2 consumption rate (nmol/g.s) with adherent temperature in CO_2 hydrogenation reaction*

Catalysts	Temperature (K)	Maximum CO_2 consumption rate (nmol/g.s)
CeO_2	555.5	1058.96
Pt/CeO_2	648	2106.14
MnO_2	473	206.06
Pt/MnO_2	665.5	8353.49
In_2O_3	665.5	683.49
Pt/In_2O_3	665.5	1371.72
NiO	638	16767.55
Pt/NiO	638	12038.21
Co_3O_4	665.5	10689.22
Pt/Co_3O_4	648	13007.98
Pt/SBA-15	648	294.11

Fig. 8 (a) and Table 4. show the selectivity values of the CO_2 hydrogenation toward CH_4 as a function of reaction temperature. CH_4 selectivity of NiO, Pt/NiO, Co_3O_4 and Pt/Co_3O_4 was 100%, 100%, 93.06%, and 100%, respectively at 473 K. Both Pt-free and Pt promoted NiO and Co_3O_4 showed almost similar selectivity towards CH_4. Ouyang et al found that CH_4 selectivity was higher over cobalt catalyst due to the presence of metallic Co under reaction condition which had strong hydrogenation ability [106]. However, pure CeO_2, MnO_2, In_2O_3

and Pt promoted CeO_2, MnO_2, In_2O_3 and SBA-15 showed zero selectivity at lower temperatures (i.e. 473 K and 573 K) and CeO_2, Pt/CeO_2 showed slightly increased selectivity at higher temperature (i.e. at 673 K).

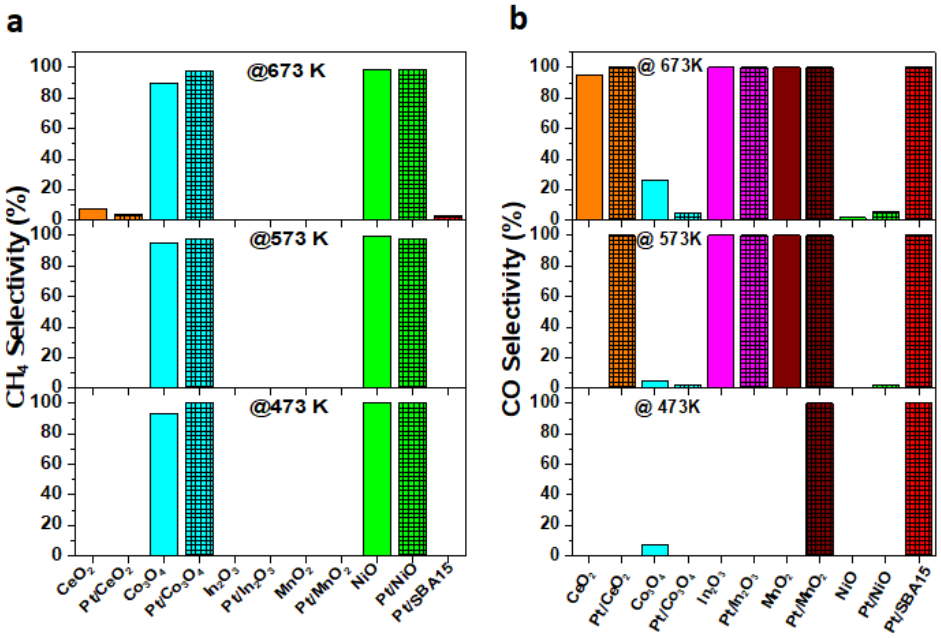

Fig. 8. *Selectivity towards (a) CH_4 and (b) CO at 473 K, 573 K and 673 K*

Fig. 8 (b) and Table 4. show CO selectivity of the catalysts. Pure CeO_2 does not show any activity thus selectivity at low temperatures (i.e. 473 and 573 K). However, it displayed 95 % selectivity at 673 K. The high CO selectivity at 673K may be due to the operation of RWGS reaction [107]. Pt/CeO_2 shows no selectivity at 473 K however, 100% selectivity was observed at 573 K and 673 K. This is due to the presence of highly reduced platinum and Ce^{3+} ions in the Pt/CeO_2 catalysts. A similar trend was observed in CuO/CeO_2 catalyst [108]. Similar behaviour was observed for Pt-free and Pt promoted MnO_2 and In_2O_3 catalysts. However, pure and Pt promoted NiO and Co_3O_4 show less CO selectivity. Pt promoted SBA-15 showed 100% selectivity towards CO. In general, both Ni- and Co-based catalysts are the most active catalysts as well as they promotes CH_4 selectivity rather than CO in the CO_2 hydrogenation reaction at 473-673 K as observed in earlier studies [109].

Table 4. *Catalytic performances over different catalysts for CO_2 hydrogenation*

Catalyst	Temperature (K)	Conversion %	Selectivity %					
			CO			CH_4		
			473 K	573 K	673 K	473 K	573 K	673 K
CeO_2	665.5	0.69	0.0000	0.0000	95.154	0.0000	0.0000	7.4848
Pt/CeO_2	648	5.08	0.0000	100.00	100.00	0.0000	0.0000	3.3994
MnO_2	665.5	0.15	0.0000	100.00	100.00	0.0000	0.0000	0.0000
Pt/MnO_2	648	25.3	100.00	100.00	100.00	0.0000	0.0000	0.0000
In_2O_3	665.5	3.89	0.0000	100.00	100.00	0.0000	0.0000	0.0000
Pt/In_2O_3	648	5.82	0.0000	100.00	100.00	0.0000	0.0000	0.0000
NiO	665.5	80.66	0.0000	0.4862	1.6314	100.00	99.513	98.440
Pt/NiO	648	78.96	0.0000	2.4043	5.1445	100.00	97.595	98.378
Co_3O_4	665.5	58.48	6.9356	4.6151	26.520	93.064	95.384	89.818
Pt/Co_3O_4	648	85.64	0.0000	2.4043	4.8735	100.00	97.595	97.622
Pt/SBA-15	673	3.15	100.00	100.00	100.00	0.0000	0.0000	2.4907

3.5.2. Dry reforming of CO_2 with methane

The performance of the catalysts was also evaluated for dry reforming reaction with a CH_4:CO_2 ratio of 1:1 in the temperature range of 473-673 K. The conversion as well as the consumption rate of CO_2 and CH_4 over different catalysts are shown in Fig. 9. and Fig. 10. respectively. CH_4 and CO_2 were converted to syngas with no noticeable by-products (e.g., alkane and alkene). The CO_2 and CH_4 conversions increased with increasing reaction temperature, as the DRM reaction is endothermic in nature. The comparison was made between the pristine supports and supports loaded with 0.5 % platinum nanoparticles. We observed in almost all reactions that platinum metal loaded support showed higher conversion compared to pristine mesoporous metal-oxides. This can be attributed to the synergetic metal support interaction as well as the high C-O and C-H breaking affinity of the Pt. Conversion of CH_4 is almost similar to CO_2 conversion for most of the catalysts, however in the case of pure NiO the conversion of CO_2 is greater than CH_4, which is showing the presence of a C-H activation favouring catalysts.

The CO_2 and CH_4 conversions increased with increasing reaction temperature, as the DRM reaction is endothermic in nature. The bare CeO_2 does not show any activity in DRM reaction. The activities of the catalysts can be ranked as NiO > Pt/Co_3O_4 > Pt/NiO > Co_3O_4 > Pt/CeO_2 > Pt/In_2O_3 > Pt/MnO_2 > In_2O_3 > MnO_2 > CeO_2. Pt-free NiO showed the highest performance among the tested catalysts with the high CH_4 conversion (65.03%) and CO_2

conversion (39.3%). The high conversion efficiency of NiO compared to other catalysts is ascribed to the formation of metallic Ni under reaction conditions resulted in a Ni/NiO_x structure, which promotes the thermal decomposition of CH_4 as it was observed in the case of CO_2 hydrogenation reaction. The expected promotion effect of Pt was also unobservable in dry reforming of CO_2.

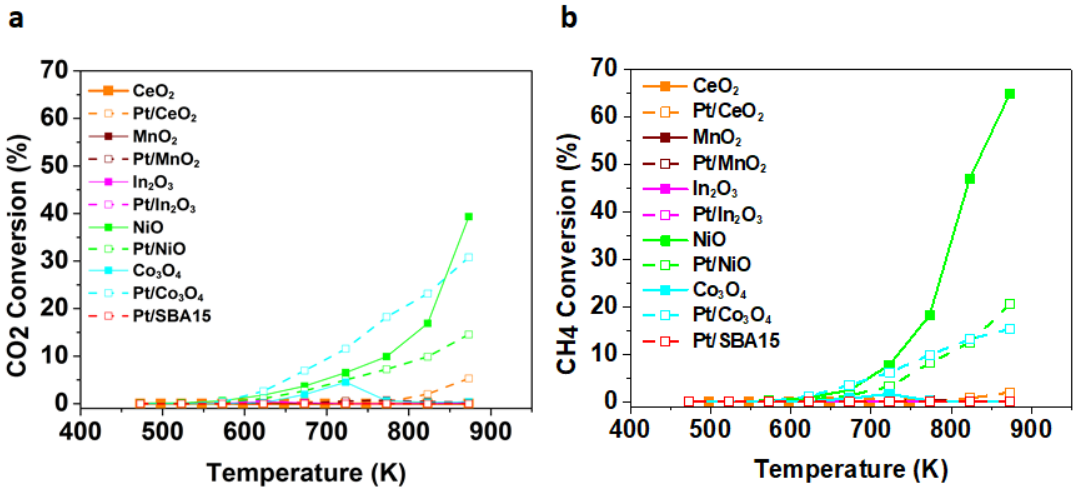

Fig. 9. *(a) CO_2 and (b) CH_4 conversion of dry reforming of CO_2 with methane over Pt-free and Pt-loaded mesoporous oxide catalysts as a function of temperature*

0.5 % Pt/Co_3O_4 catalysts showed amazingly higher CO_2 (30.8%) and CH_4 (15.3%) conversion compared to pure Co_3O_4 (0.38% CO_2 conversion and 0.14% CH_4 conversion). This is due to the presence of Pt^0 and Co^0 species as well as a special synergetic of Pt/Co/CoOx structure in Pt/Co_3O_4. Besides, the presence of Pt^0 which was found to have higher hydrogen dissociation ability is responsible for the higher CO_2 and CH_4 conversion in contrast to Co_3O_4 in which only Co^0 species are present [110].

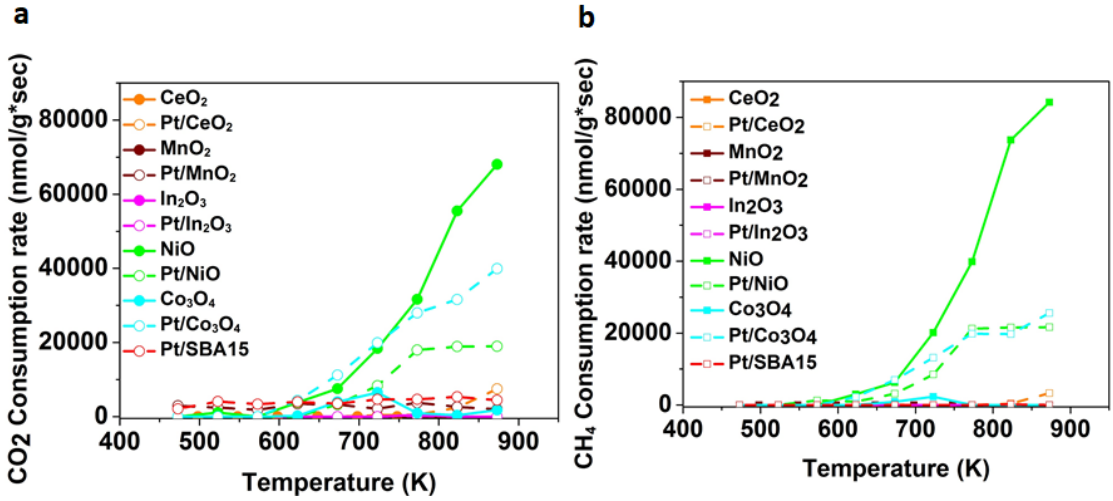

Fig. 10. *Consumption rate of (a) CO_2 and (b) CH_4 of dry reforming of CO_2 with methane over Pt-free and Pt-loaded mesoporous oxide catalysts as a function of temperature*

The maximum CO_2 consumption rate of all catalysts can be seen in Table 5. We can see that the CO_2 consumption rate was much greater on NiO compared to other pure or Pt promoted catalysts. This activity is competing well with other catalyts used in dry refomring of CO_2 with methane [69, 111] .

Table 6. *The maximum CO_2 consumption rate (nmol/g.s)*

Catalysts	Temperature (K)	Maximum CO_2 consumption rate (nmol/g.s)
CeO_2	473-873	0
Pt/CeO_2	873	7475.62
MnO_2	773	1596.58
Pt/MnO_2	623	3459.09
In_2O_3	773	436.21
Pt/In_2O_3	773	171.25
NiO	873	68036.13
Pt/NiO	873	18963.52
Co_3O_4	723	6457.78
Pt/Co_3O_4	823	39935.44
Pt/SBA-15	823	5324.80

Fig. 11. compares the H_2/CO ratio in the temperature range of 673-973 K for dry reforming of CO_2 with methane over the mesoporous oxide-based catalysts. The H_2/CO ratio

is generally higher at high temperature, which is due to the occurrence of carbon gasification, methane decomposition, and water-gas shift reaction, which produces H_2. The H_2/CO ratio was between 0 and 2.2 over the entire range of temperature studied (673 – 973 K). The values of H_2/CO ratio were found to be less than unity notably at low temperature. This can be attributed to the occurrence of RWGS and methanation reactions at low temperatures, which consumes H_2. The ratio decreases at higher temperatures (at 873 and 973 K) which may be due to the sintering of metal particles as well as the carbon deposition [112]. As the temperature increases further, the DRM reaction become significant as per the thermodynamic point of view. However, Pt/SBA-15 displayed almost zero H_2/CO ratio at low temperatures (673 K, 773K and 873 K) but it displays higher H_2/CO ratio (2.2) at 973 K. This may be due to the oxidation of carbon deposition by the platinum metal that is well dispersed on the high surface area SBA-15 support [113]. However, the activity of Pt/SBA-15 catalysts was really low. On the other hand, pure NiO catalyst show H_2/CO ratio of close to the optimal unity value showing the presence of a highly active and selective catalyst.

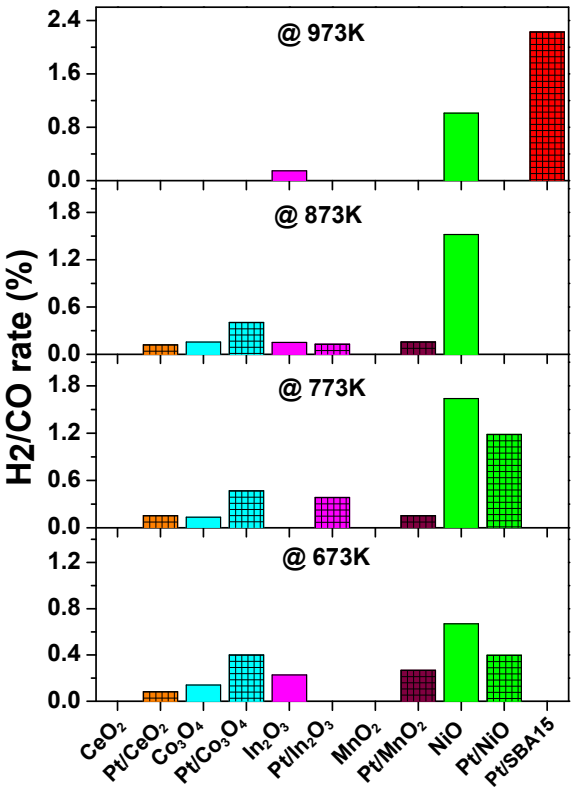

Fig. 11. *Effect of temperature on H_2/CO ratio for various catalysts in dry reforming of CO_2*

3.7 Post-reaction catalyst properties

The crystal structures of the used catalysts after CO_2 hydrogenation reaction were investigated by XRD. The diffraction patterns obtained for the used catalysts along with as-prepared catalysts are presented in Fig. 12. and Fig. 13 for CO_2 hydrogenation and CO_2 methanation respectively. The peak intensity in the XRD pattern of spent CeO_2 increased compared to the fresh catalyst which may be due to partial sintering of the catalysts under the experimental conditions [114]. However, MnO_2, In_2O_3, NiO, and Co_3O_4 present new peaks after reactions showing the phase transition of the supports under reaction conditions. The spent MnO_2 catalyst shows peaks at 2θ = 35°, 40.7°, 58.7°, 70.2° and 73.8° can be indexed to (111), (200), (220), (311) and (222) planes respectively of MnO phase (JCPDS No.78-0424) [115] with less intense peaks at 32.5°, 36.09°, 44.3°, 51.2° and can be indexed to the (103), (211), (220) and (105) planes of Mn_3O_4 (JCPDS No. 24-0734) tetragonal phase. The spent In_2O_3 shows peaks at 32.9°, 39.1° and 54.4° can be indexed to (011), (110) and (112) planes respectively of tetragonal phase of metallic indium (JCPDS No. 05-0642) [116]. The spent NiO show peaks at 2θ = 44.5°, 51.8° and 76.3° can be indexed to (111), (200) and (220) planes respectively for metallic nickel (JCPDS No. 65-2865) [117]. The spent Co_3O_4 catalyst shows peaks at 2θ = 44.2°, 51.5° and 75.9° can be indexed to (111), (200) and (220) planes of metallic cobalt (JCPDS No. 05-0727) [118].

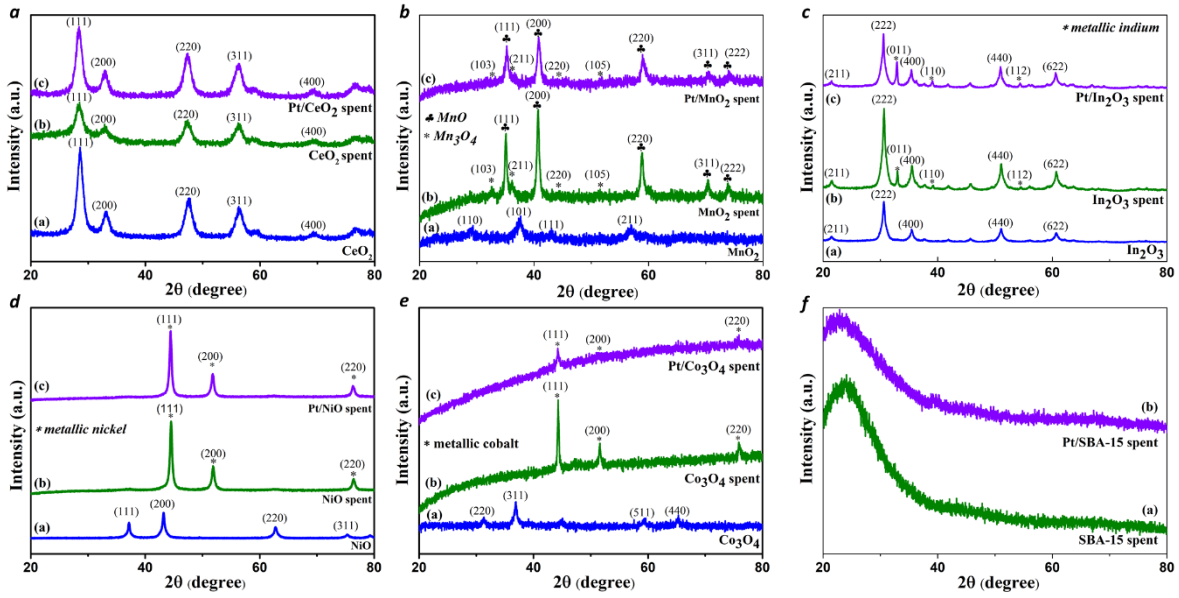

Fig. 12. *XRD patterns of fresh as well as spent Pt-free and Pt-loaded supports (a) CeO_2 (b) MnO_2 (c) In_2O_3 (d) NiO (e) Co_3O_4 (f) SBA-15 after CO_2 hydrogenation.*

The diffraction patterns obtained for the used catalysts after dry reforming of CO_2 with methane along with fresh catalysts are presented in Fig. 13. The spent catalysts after DRM reaction showed similar XRD pattern as that of the spent catalyst obtained from CO_2 hydrogenation reaction except that the intensities of peaks are weak. The presence of Mn_3O_4 in MnO_2, metallic Ni in NiO and metallic Co in Co_3O_4 under reaction conditions are responsible for their higher catalytic activities in both CO_2 hydrogenation and DRM reactions.

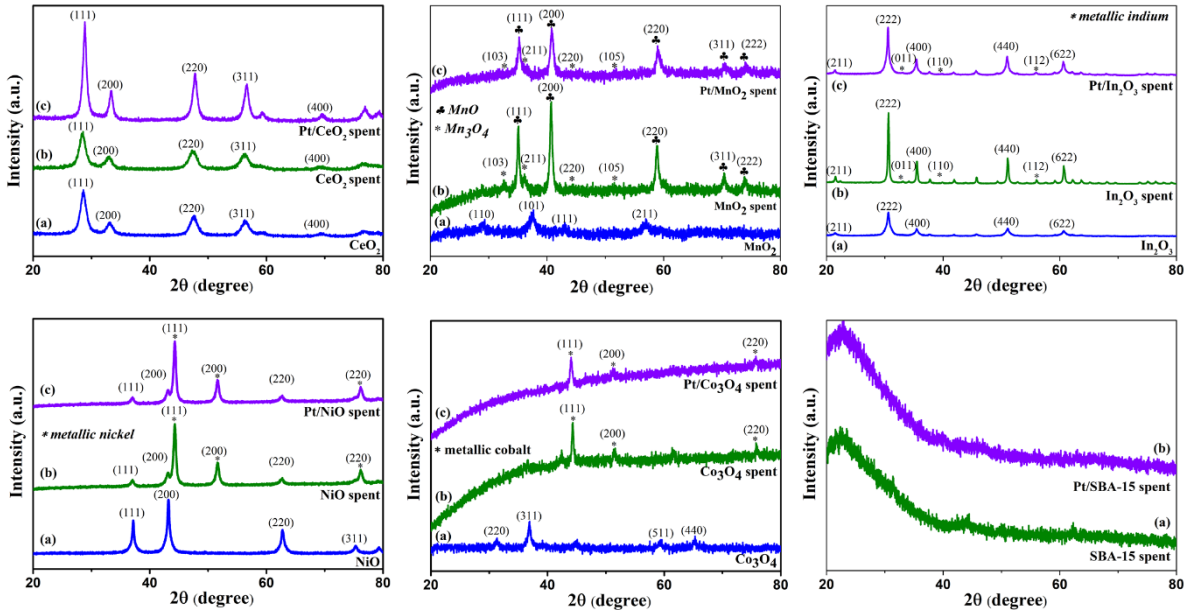

Fig. 13. *XRD patterns of fresh as well as spent Pt-free and Pt-loaded supports (a) CeO_2 (b) MnO_2 (c) In_2O_3 (d) NiO (e) Co_3O_4 (f) SBA-15 after DRM reaction*

4. Conclusions

In this study, a series of mesoporous metal oxides such as CeO_2, MnO_2, In_2O_3, NiO, and Co_3O_4 were prepared by hard template method. Pt nanoparticles of 4.8 nm were dispersed on the surface of these mesoporous oxides. The H_2-TPR profiles show a decrease of reduction temperature for the mesoporous oxides supported Pt compared to that of pure supports which can be attributed to the spillover of H_2 form Pt to supports. Nickel-oxide and Cobalt-oxide based catalysts showed the best performance in CO_2 activation reactions.

Pt-free NiO exhibited the highest catalytic activity for both CO_2 hydrogenation and methanation reactions. The enhanced catalytic properties can be ascribed to the presence of metallic Ni and the optimal concentration of Ni/NiO_x under reaction conditions. In the case of cobalt based catalysts, Pt/Co_3O_4 showed higher catalytic activity than the corresponding Co_3O_4 mesoporous structures for both CO_2 activation reactions. The high catalytic activities of

Pt/Co_3O_4 resulted from the presence of metallic cobalt, Pt nanoparticles as well as synergistic effect between the Pt and Co_3O_4 mesoporous structures.

The results presented in this study show the importance of the nature of oxide supports as well as the significance of formed interphases under reaction conditions. The presence of Pt nanoparticles is not sufficient in certain cases. The efficiency of Pt supported oxide catalyst determined not only reducibility of oxide support but also the character of formed interfaces. Dynamically different Ni/NiO, Pt/Ni/NiO, $Pt/Co/Co_3O_4$ interfaces could be built up during the reduction step which determine the activity and selectivity in both reactions. In the future, noble-metal free catalysts will be tested where the optimal metal/metal-oxide structure will be prepared for the high activity and selectivity reactions.

Acknowledgement

This paper was supported by the Hungarian Research Development and Innovation Office through grants NKFIH OTKA PD 120877 of AS. ÁK, and KZ is grateful for the fund of NKFIH (OTKA) K112531 & NN110676 and K120115, respectively. The financial support of the Hungarian National Research, Development and Innovation Office through the GINOP-2.3.2-15-2016-00013 project "Intelligent materials based on functional surfaces - from syntheses to applications" and the Ministry of Human Capacities through the EFOP-3.6.1-16-2016-00014 project is acknowledged.

Author Information

Corresponding Author

* sapia@chem.u-szeged.hu

References

[1] Z.Z. Noor, R.O. Yusuf, A.H. Abba, M.A.A. Hassan, M.F.M. Din, An overview for energy recovery from municipal solid wastes (MSW) in Malaysia scenario, Renewable and Sustainable Energy Reviews 20 (2013) 378-384.
[2] W. Wang, S. Wang, X. Ma, J. Gong, Recent advances in catalytic hydrogenation of carbon dioxide, Chemical Society Reviews 40(7) (2011) 3703-3727.
[3] S. Kattel, P. Liu, J.G. Chen, Tuning Selectivity of CO2 Hydrogenation Reactions at the Metal/Oxide Interface, Journal of the American Chemical Society 139(29) (2017) 9739-9754.

[4] F. Studt, I. Sharafutdinov, F. Abild-Pedersen, C.F. Elkjær, J.S. Hummelshøj, S. Dahl, I. Chorkendorff, J.K. Nørskov, Discovery of a Ni-Ga catalyst for carbon dioxide reduction to methanol, Nature chemistry 6(4) (2014) 320.
[5] S. Kattel, P.J. Ramírez, J.G. Chen, J.A. Rodriguez, P. Liu, Active sites for CO2 hydrogenation to methanol on Cu/ZnO catalysts, Science 355(6331) (2017) 1296-1299.
[6] M.D. Porosoff, J.G. Chen, Trends in the catalytic reduction of CO2 by hydrogen over supported monometallic and bimetallic catalysts, Journal of catalysis 301 (2013) 30-37.
[7] R.W. Dorner, D.R. Hardy, F.W. Williams, H.D. Willauer, Heterogeneous catalytic CO 2 conversion to value-added hydrocarbons, Energy & Environmental Science 3(7) (2010) 884-890.
[8] F. Schneck, J. Ahrens, M. Finger, A.C. Stückl, C. Würtele, D. Schwarzer, S. Schneider, The elusive abnormal CO 2 insertion enabled by metal-ligand cooperative photochemical selectivity inversion, Nature communications 9(1) (2018) 1161.
[9] M. Ronda-Lloret, S. Rico-Francés, A. Sepúlveda-Escribano, E.V. Ramos-Fernandez, CuOx/CeO 2 catalyst derived from Metal Organic Framework for Reverse Water-Gas Shift Reaction, Applied Catalysis A: General (2018).
[10] S. Choi, B.-I. Sang, J. Hong, K.J. Yoon, J.-W. Son, J.-H. Lee, B.-K. Kim, H. Kim, Catalytic behavior of metal catalysts in high-temperature RWGS reaction: In-situ FT-IR experiments and first-principles calculations, Scientific reports 7 (2017) 41207.
[11] X. Zhao, H. Xu, X. Wang, Z. Zheng, Z. Xu, J. Ge, Monodisperse metal–organic framework nanospheres with encapsulated core–shell nanoparticles Pt/Au@ Pd@{Co2 (oba) 4 (3-bpdh) 2} 4H2O for the highly selective conversion of CO2 to CO, ACS applied materials & interfaces 10(17) (2018) 15096-15103.
[12] X. Chen, X. Su, H. Duan, B. Liang, Y. Huang, T. Zhang, Catalytic performance of the Pt/TiO2 catalysts in reverse water gas shift reaction: Controlled product selectivity and a mechanism study, Catalysis today 281 (2017) 312-318.
[13] X. Yang, X. Su, X. Chen, H. Duan, B. Liang, Q. Liu, X. Liu, Y. Ren, Y. Huang, T. Zhang, Promotion effects of potassium on the activity and selectivity of Pt/zeolite catalysts for reverse water gas shift reaction, Applied Catalysis B: Environmental 216 (2017) 95-105.
[14] S. Kattel, B. Yan, J.G. Chen, P. Liu, CO 2 hydrogenation on Pt, Pt/SiO 2 and Pt/TiO 2: Importance of synergy between Pt and oxide support, Journal of Catalysis 343 (2016) 115-126.
[15] X. Wang, H. Shi, J.H. Kwak, J. Szanyi, Mechanism of CO2 Hydrogenation on Pd/Al2O3 Catalysts: Kinetics and Transient DRIFTS-MS Studies, ACS Catalysis 5(11) (2015) 6337-6349.
[16] S. Bebelis, H. Karasali, C.G. Vayenas, Electrochemical promotion of the CO2 hydrogenation on Pd/YSZ and Pd/β″-Al2O3 catalyst-electrodes, Solid State Ionics 179(27) (2008) 1391-1395.
[17] F. Solymosi, A. Erdöhelyi, M. Lancz, Surface interaction between H2 and CO2 over palladium on various supports, Journal of Catalysis 95(2) (1985) 567-577.
[18] A. Erdöhelyi, M. Pásztor, F. Solymosi, Catalytic hydrogenation of CO2 over supported palladium, Journal of Catalysis 98(1) (1986) 166-177.
[19] S.V. Lambeets, C. Barroo, S. Owczarek, L. Jacobs, E. Genty, N. Gilis, N. Kruse, T. Visart de Bocarmé, Adsorption and Hydrogenation of CO2 on Rh Nanosized Crystals: Demonstration of the Role of Interfacet Oxygen Spillover and Comparative Studies with O2, N2O, and CO, The Journal of Physical Chemistry C 121(30) (2017) 16238-16249.
[20] Z. Cao, L. Guo, N. Liu, X. Zheng, W. Li, Y. Shi, J. Guo, Y. Xi, Theoretical study on the reaction mechanism of reverse water-gas shift reaction using a Rh-Mo6S8 cluster, RSC Advances 6(110) (2016) 108270-108279.

[21] F. Solymosi, A. Erdöhelyi, T. Bánsági, Infrared study of the surface interaction between H 2 and CO 2 over rhodium on various supports, Journal of the Chemical Society, Faraday Transactions 1: Physical Chemistry in Condensed Phases 77(11) (1981) 2645-2657.
[22] I.A. Fisher, A.T. Bell, A Comparative Study of CO and CO2Hydrogenation over Rh/SiO2, Journal of catalysis 162(1) (1996) 54-65.
[23] M. Tóth, J. Kiss, A. Oszkó, G. Pótári, B. László, A. Erdőhelyi, Hydrogenation of Carbon Dioxide on Rh, Au and Au–Rh Bimetallic Clusters Supported on Titanate Nanotubes, Nanowires and TiO2, Topics in Catalysis 55(11) (2012) 747-756.
[24] Á. Kukovecz, K. Kordás, J. Kiss, Z. Kónya, Atomic scale characterization and surface chemistry of metal modified titanate nanotubes and nanowires, Surface Science Reports 71(3) (2016) 473-546.
[25] V. Kyriakou, A. Vourros, I. Garagounis, S.A.C. Carabineiro, F.J. Maldonado-Hódar, G.E. Marnellos, M. Konsolakis, Highly active and stable TiO2-supported Au nanoparticles for CO2 reduction, Catalysis Communications 98 (2017) 52-56.
[26] I. Ro, R. Carrasquillo-Flores, J.A. Dumesic, G.W. Huber, Intrinsic kinetics of plasmon-enhanced reverse water gas shift on Au and Au–Mo interfacial sites supported on silica, Applied Catalysis A: General 521 (2016) 182-189.
[27] F. Solymosi, A. Erdöhelyi, M. Kocsis, Methanation of CO 2 on supported Ru catalysts, Journal of the Chemical Society, Faraday Transactions 1: Physical Chemistry in Condensed Phases 77(5) (1981) 1003-1012.
[28] L. Lin, S. Yao, Z. Liu, F. Zhang, N. Li, D. Vovchok, A. Martínez-Arias, R. Castañeda, J. Lin, S.D. Senanayake, D. Su, D. Ma, J.A. Rodriguez, In Situ Characterization of Cu/CeO2 Nanocatalysts for CO2 Hydrogenation: Morphological Effects of Nanostructured Ceria on the Catalytic Activity, The Journal of Physical Chemistry C 122(24) (2018) 12934-12943.
[29] E.L. Fornero, D.L. Chiavassa, A.L. Bonivardi, M.A. Baltanás, Transient analysis of the reverse water gas shift reaction on Cu/ZrO2 and Ga2O3/Cu/ZrO2 catalysts, Journal of CO2 Utilization 22 (2017) 289-298.
[30] X. Liu, P. Ramírez de la Piscina, J. Toyir, N. Homs, CO2 reduction over Cu-ZnGaMO (M=Al, Zr) catalysts prepared by a sol-gel method: Unique performance for the RWGS reaction, Catalysis Today 296 (2017) 181-186.
[31] L. Pastor-Pérez, F. Baibars, E. Le Sache, H. Arellano-García, S. Gu, T.R. Reina, CO2 valorisation via Reverse Water-Gas Shift reaction using advanced Cs doped Fe-Cu/Al2O3 catalysts, Journal of CO2 Utilization 21 (2017) 423-428.
[32] J.A. Loiland, M.J. Wulfers, N.S. Marinkovic, R.F. Lobo, Fe/[gamma]-Al2O3 and Fe-K/[gamma]-Al2O3 as reverse water-gas shift catalysts, Catalysis Science & Technology 6(14) (2016) 5267-5279.
[33] L. Yang, L. Pastor-Pérez, S. Gu, A. Sepúlveda-Escribano, T.R. Reina, Highly efficient Ni/CeO2-Al2O3 catalysts for CO2 upgrading via reverse water-gas shift: Effect of selected transition metal promoters, Applied Catalysis B: Environmental 232 (2018) 464-471.
[34] P. Marocco, E.A. Morosanu, E. Giglio, D. Ferrero, C. Mebrahtu, A. Lanzini, S. Abate, S. Bensaid, S. Perathoner, M. Santarelli, R. Pirone, G. Centi, CO2 methanation over Ni/Al hydrotalcite-derived catalyst: Experimental characterization and kinetic study, Fuel 225 (2018) 230-242.
[35] M. Ronda-Lloret, S. Rico-Francés, A. Sepúlveda-Escribano, E.V. Ramos-Fernandez, CuOx/CeO2 catalyst derived from metal organic framework for reverse water-gas shift reaction, Applied Catalysis A: General 562 (2018) 28-36.
[36] C. Panaritis, M. Edake, M. Couillard, R. Einakchi, E.A. Baranova, Insight towards the role of ceria-based supports for reverse water gas shift reaction over RuFe nanoparticles, Journal of CO2 Utilization 26 (2018) 350-358.

[37] B.J. Hare, D. Maiti, Y.A. Daza, V.R. Bhethanabotla, J.N. Kuhn, Enhanced CO2 Conversion to CO by Silica-Supported Perovskite Oxides at Low Temperatures, ACS Catalysis 8(4) (2018) 3021-3029.
[38] I. Ro, C. Sener, T.M. Stadelman, M.R. Ball, J.M. Venegas, S.P. Burt, I. Hermans, J.A. Dumesic, G.W. Huber, Measurement of intrinsic catalytic activity of Pt monometallic and Pt-MoOx interfacial sites over visible light enhanced PtMoOx/SiO2 catalyst in reverse water gas shift reaction, Journal of Catalysis 344 (2016) 784-794.
[39] K. Zhao, Q. Bkour, X. Hou, S.W. Kang, J.C. Park, M.G. Norton, J.-I. Yang, S. Ha, Reverse water gas shift reaction over CuFe/Al2O3 catalyst in solid oxide electrolysis cell, Chemical Engineering Journal 336 (2018) 20-27.
[40] N. Kanjanasoontorn, T. Permsirivanich, T. Numpilai, T. Witoon, N. Chanlek, M. Niamlaem, C. Warakulwit, J. Limtrakul, Structure–Activity Relationships of Hierarchical Meso–Macroporous Alumina Supported Copper Catalysts for CO2 Hydrogenation: Effects of Calcination Temperature of Alumina Support, Catalysis Letters 146(10) (2016) 1943-1955.
[41] M. Tahir, N.A.S. Amin, Photo-induced CO2 reduction by hydrogen for selective CO evolution in a dynamic monolith photoreactor loaded with Ag-modified TiO2 nanocatalyst, International Journal of Hydrogen Energy 42(23) (2017) 15507-15522.
[42] S. Schiebahn, T. Grube, M. Robinius, V. Tietze, B. Kumar, D. Stolten, Power to gas: Technological overview, systems analysis and economic assessment for a case study in Germany, International journal of hydrogen energy 40(12) (2015) 4285-4294.
[43] F.D. Meylan, F.-P. Piguet, S. Erkman, Power-to-gas through CO2 methanation: assessment of the carbon balance regarding EU directives, Journal of Energy Storage 11 (2017) 16-24.
[44] D. Wierzbicki, R. Baran, R. Dębek, M. Motak, M.E. Gálvez, T. Grzybek, P. Da Costa, P. Glatzel, Examination of the influence of La promotion on Ni state in hydrotalcite-derived catalysts under CO2 methanation reaction conditions: Operando X-ray absorption and emission spectroscopy investigation, Applied Catalysis B: Environmental 232 (2018) 409-419.
[45] M. Bacariza, I. Graça, J. Lopes, C. Henriques, Enhanced activity of CO2 hydrogenation to CH4 over Ni based zeolites through the optimization of the Si/Al ratio, Microporous and Mesoporous Materials 267 (2018) 9-19.
[46] A. Vita, C. Italiano, L. Pino, P. Frontera, M. Ferraro, V. Antonucci, Activity and stability of powder and monolith-coated Ni/GDC catalysts for CO 2 methanation, Applied Catalysis B: Environmental (2018).
[47] G. Zhou, H. Liu, Y. Xing, S. Xu, H. Xie, K. Xiong, CO 2 hydrogenation to methane over mesoporous Co/SiO 2 catalysts: Effect of structure, Journal of CO2 Utilization 26 (2018) 221-229.
[48] X. Nie, H. Wang, W. Li, Y. Chen, X. Guo, C. Song, DFT insight into the support effect on the adsorption and activation of key species over Co catalysts for CO 2 methanation, Journal of CO2 Utilization 24 (2018) 99-111.
[49] J. Díez-Ramírez, P. Sánchez, V. Kyriakou, S. Zafeiratos, G. Marnellos, M. Konsolakis, F. Dorado, Effect of support nature on the cobalt-catalyzed CO 2 hydrogenation, Journal of CO2 Utilization 21 (2017) 562-571.
[50] S. Okada, R. Manabe, R. Inagaki, S. Ogo, Y. Sekine, Methane dissociative adsorption in catalytic steam reforming of methane over Pd/CeO2 in an electric field, Catalysis Today (2017).
[51] X. Wang, H. Shi, J.H. Kwak, J.n. Szanyi, Mechanism of CO2 hydrogenation on Pd/Al2O3 catalysts: kinetics and transient DRIFTS-MS studies, ACS Catalysis 5(11) (2015) 6337-6349.
[52] A. Petala, P. Panagiotopoulou, Methanation of CO2 over alkali-promoted Ru/TiO2 catalysts: I. Effect of alkali additives on catalytic activity and selectivity, Applied Catalysis B: Environmental 224 (2018) 919-927.

[53] A. Kim, D.P. Debecker, F. Devred, V. Dubois, C. Sanchez, C. Sassoye, CO2 methanation on Ru/TiO2 catalysts: On the effect of mixing anatase and rutile TiO2 supports, Applied Catalysis B: Environmental 220 (2018) 615-625.
[54] L. Lin, K. Wang, K. Yang, X. Chen, X. Fu, W. Dai, The visible-light-assisted thermocatalytic methanation of CO2 over Ru/TiO (2-x) Nx, Applied Catalysis B: Environmental 204 (2017) 440-455.
[55] N.M. Martin, F. Hemmingsson, X. Wang, L.R. Merte, U. Hejral, J. Gustafson, M. Skoglundh, D.M. Meira, A.-C. Dippel, O. Gutowski, Structure–function relationship during CO 2 methanation over Rh/Al 2 O 3 and Rh/SiO 2 catalysts under atmospheric pressure conditions, Catalysis Science & Technology 8(10) (2018) 2686-2696.
[56] R. Thalinger, T. Götsch, C. Zhuo, W. Hetaba, W. Wallisch, M. Stöger-Pollach, D. Schmidmair, B. Klötzer, S. Penner, Rhodium-Catalyzed Methanation and Methane Steam Reforming Reactions on Rhodium–Perovskite Systems: Metal–Support Interaction, ChemCatChem 8(12) (2016) 2057-2067.
[57] M. Mihet, M.D. Lazar, Methanation of CO2 on Ni/γ-Al2O3: influence of Pt, Pd or Rh promotion, Catalysis Today (2016).
[58] Y. Xu, Y. Chen, J. Li, J. Zhou, M. Song, X. Zhang, Y. Yin, Improved low-temperature activity of Ni–Ce/γ-Al2O3 catalyst with layer structural precursor prepared by cold plasma for CO2 methanation, International Journal of Hydrogen Energy 42(18) (2017) 13085-13091.
[59] F. Song, Q. Zhong, Y. Yu, M. Shi, Y. Wu, J. Hu, Y. Song, Obtaining well-dispersed Ni/Al2O3 catalyst for CO2 methanation with a microwave-assisted method, International Journal of Hydrogen Energy 42(7) (2017) 4174-4183.
[60] T.A. Le, J.K. Kang, E.D. Park, CO and CO 2 Methanation Over Ni/SiC and Ni/SiO 2 Catalysts, Topics in Catalysis 1-8.
[61] T.A. Le, T.W. Kim, S.H. Lee, E.D. Park, Effects of Na content in Na/Ni/SiO2 and Na/Ni/CeO2 catalysts for CO and CO2 methanation, Catalysis Today (2017).
[62] P. Schlexer, H.-Y.T. Chen, G. Pacchioni, CO2 Activation and Hydrogenation: A Comparative DFT Study of Ru10/TiO2 and Cu10/TiO2 Model Catalysts, Catalysis Letters 147(8) (2017) 1871-1881.
[63] P. Panagiotopoulou, X.E. Verykios, Mechanistic Study of the Selective Methanation of CO over Ru/TiO2 Catalysts: Effect of Metal Crystallite Size on the Nature of Active Surface Species and Reaction Pathways, The Journal of Physical Chemistry C 121(9) (2017) 5058-5068.
[64] Y. Guo, S. Mei, K. Yuan, D.-J. Wang, H. Liu, C.-H. Yan, Y.-W. Zhang, Low-Temperature CO2 Methanation over CeO2-Supported Ru Single Atoms, Nanoclusters and Nanoparticles Competitively Tuned by Strong Metal-Support Interactions and H-Spillover Effect, ACS Catalysis (2018).
[65] A. Sápi, G. Halasi, J. Kiss, D.G. Dobó, K.n.L. Juhász, V.J. Kolcsár, Z. Ferencz, G. Vári, V. Matolin, A.s. Erdőhelyi, In Situ DRIFTS and NAP-XPS Exploration of the Complexity of CO2 Hydrogenation over Size-Controlled Pt Nanoparticles Supported on Mesoporous NiO, The Journal of Physical Chemistry C 122(10) (2018) 5553-5565.
[66] Y. Zhou, Y. Jiang, Z. Qin, Q. Xie, H. Ji, Influence of Zr, Ce, and La on Co3O4 catalyst for CO2 methanation at low temperature, Chinese Journal of Chemical Engineering (2017).
[67] O. Muraza, A. Galadima, A review on coke management during dry reforming of methane, International Journal of Energy Research 39(9) (2015) 1196-1216.
[68] G.S. Gallego, C. Batiot-Dupeyrat, J. Barrault, E. Florez, F. Mondragon, Dry reforming of methane over LaNi1− yByO3±δ (B= Mg, Co) perovskites used as catalyst precursor, Applied Catalysis A: General 334(1-2) (2008) 251-258.

[69] H.Y. Kim, J.N. Park, G. Henkelman, J.M. Kim, Design of a Highly Nanodispersed Pd–MgO/SiO2 Composite Catalyst with Multifunctional Activity for CH4 Reforming, ChemSusChem 5(8) (2012) 1474-1481.
[70] D. Pakhare, J. Spivey, A review of dry (CO 2) reforming of methane over noble metal catalysts, Chemical Society Reviews 43(22) (2014) 7813-7837.
[71] M.C.J. Bradford, M.A. Vannice, CO2 Reforming of CH4, Catalysis Reviews 41(1) (1999) 1-42.
[72] F. Solymosi, G. Kutsan, A. Erdöhelyi, Catalytic reaction of CH 4 with CO 2 over alumina-supported Pt metals, Catalysis Letters 11(2) (1991) 149-156.
[73] I. Sarusi, K. Fodor, K. Baán, A. Oszkó, G. Pótári, A. Erdőhelyi, CO2 reforming of CH4 on doped Rh/Al2O3 catalysts, Catalysis Today 171(1) (2011) 132-139.
[74] E. Varga, P. Pusztai, L. Óvári, A. Oszkó, A. Erdőhelyi, C. Papp, H.-P. Steinrück, Z. Kónya, J. Kiss, Probing the interaction of Rh, Co and bimetallic Rh–Co nanoparticles with the CeO 2 support: catalytic materials for alternative energy generation, Physical Chemistry Chemical Physics 17(40) (2015) 27154-27166.
[75] C.j. Liu, J. Ye, J. Jiang, Y. Pan, Progresses in the Preparation of Coke Resistant Ni-Based Catalyst for Steam and CO2 Reforming of Methane, ChemCatChem 3(3) (2011) 529-541.
[76] A.A. Ibrahim, M.A. Naeem, A.H. Fakeeha, W.U. Khan, A.S. Al-Fatesh, A.E. Abasaeed, Production of Synthesis Gas via Dry Reforming of Methane over Co-Based Catalysts: Effect on H2/CO Ratio and Carbon Deposition, Chemical Engineering & Technology 38(8) (2015) 1397-1405.
[77] V.M. Gonzalez-Delacruz, R. Pereñiguez, F. Ternero, J.P. Holgado, A. Caballero, Modifying the size of nickel metallic particles by H2/CO treatment in Ni/ZrO2 methane dry reforming catalysts, Acs Catalysis 1(2) (2011) 82-88.
[78] J. Károlyi, M. Németh, C. Evangelisti, G. Sáfrán, Z. Schay, A. Horváth, F. Somodi, Carbon dioxide reforming of methane over Ni–In/SiO2 catalyst without coke formation, Journal of Industrial and Engineering Chemistry 58 (2018) 189-201.
[79] Z. Xie, B. Yan, S. Kattel, J.H. Lee, S. Yao, Q. Wu, N. Rui, E. Gomez, Z. Liu, W. Xu, Dry Reforming of Methane over CeO 2-supported Pt-Co Catalysts with Enhanced Activity, Applied Catalysis B: Environmental (2018).
[80] M. Wang, T. Zhao, X. Dong, M. Li, H. Wang, Effects of Ce substitution at the A-site of LaNi0. 5Fe0. 5O3 perovskite on the enhanced catalytic activity for dry reforming of methane, Applied Catalysis B: Environmental 224 (2018) 214-221.
[81] F.R. Shamskar, F. Meshkani, M. Rezaei, Preparation and characterization of ultrasound-assisted co-precipitated nanocrystalline La-, Ce-, Zr–promoted Ni-Al2O3 catalysts for dry reforming reaction, Journal of CO2 Utilization 22 (2017) 124-134.
[82] H. Zhang, M. Li, P. Xiao, D. Liu, C.-J. Zou, Structure and Catalytic Performance of Mg-SBA-15-Supported Nickel Catalysts for CO2 Reforming of Methane to Syngas, Chemical Engineering & Technology 36(10) (2013) 1701-1707.
[83] K. An, S. Alayoglu, N. Musselwhite, S. Plamthottam, G.r.m. Melaet, A.E. Lindeman, G.A. Somorjai, Enhanced CO oxidation rates at the interface of mesoporous oxides and Pt nanoparticles, Journal of the American Chemical Society 135(44) (2013) 16689-16696.
[84] K.S. Sing, Reporting physisorption data for gas/solid systems with special reference to the determination of surface area and porosity (Recommendations 1984), Pure and applied chemistry 57(4) (1985) 603-619.
[85] C. Rotaru, G. Postole, M. Florea, F. Matei-Rutkovska, V. Pârvulescu, P. Gelin, Dry reforming of methane on ceria prepared by modified precipitation route, Applied Catalysis A: General 494 (2015) 29-40.

[86] H. Liu, Z. Hu, Y. Su, H. Ruan, R. Hu, L. Zhang, MnO2 nanorods/3D-rGO composite as high performance anode materials for Li-ion batteries, Applied Surface Science 392 (2017) 777-784.
[87] D. Pan, S. Ge, X. Zhang, X. Mai, S. Li, Z. Guo, Synthesis and photoelectrocatalytic activity of In 2 O 3 hollow microspheres via a bio-template route using yeast templates, Dalton Transactions 47(3) (2018) 708-715.
[88] G. Rajeshkhanna, G.R. Rao, Micro and nano-architectures of Co3O4 on Ni foam for electro-oxidation of methanol, International Journal of Hydrogen Energy (2017).
[89] Y. Ma, X. Wang, X. Sun, T. Gao, Y. Liu, L. Zhang, Q. Huo, Z.-A. Qiao, Core–shell structured hierarchically porous NiO microspheres with enhanced electrocatalytic activity for oxygen evolution reaction, Inorganic Chemistry Frontiers 5(5) (2018) 1199-1206.
[90] T.J. Siang, T.L. Pham, N. Van Cuong, P.T. Phuong, N.H.H. Phuc, Q.D. Truong, D.-V.N. Vo, Combined steam and CO2 reforming of methane for syngas production over carbon-resistant boron-promoted Ni/SBA-15 catalysts, Microporous and Mesoporous Materials 262 (2018) 122-132.
[91] S. Brunauer, L.S. Deming, W.E. Deming, E. Teller, On a theory of the van der Waals adsorption of gases, Journal of the American Chemical society 62(7) (1940) 1723-1732.
[92] Y. Lei, W. Li, Q. Liu, Q. Lin, X. Zheng, Q. Huang, S. Guan, X. Wang, C. Wang, F. Li, Typical crystal face effects of different morphology ceria on the activity of Pd/CeO 2 catalysts for lean methane combustion, Fuel 233 (2018) 10-20.
[93] M.M. Makhlouf, Preparation and optical characterization of β-MnO2 nano thin films for application in heterojunction photodiodes, Sensors and Actuators A: Physical 279 (2018) 145-156.
[94] S. Shi, F. Zhang, H. Lin, Q. Wang, E. Shi, F. Qu, Enhanced triethylamine-sensing properties of PN heterojunction Co3O4/In2O3 hollow microtubes derived from metal–organic frameworks, Sensors and Actuators B: Chemical 262 (2018) 739-749.
[95] H. Gao, Q. Yu, S. Zhang, T. Wang, P. Sun, H. Lu, F. Liu, X. Yan, F. Liu, X. Liang, Nanosheet-assembled NiO microspheres modified by Sn2+ ions isovalent interstitial doping for xylene gas sensors, Sensors and Actuators B: Chemical 269 (2018) 210-222.
[96] K. Zhang, J. Zhang, L. Ma, Y. Liang, X. Yang, Z. Cui, S. Zhu, Z. Li, The controllable preparation of Co3O4 nanostructure for designing optimal mechanical and magnetic properties of graphite/kaolin based compounds, Materials & Design 143 (2018) 169-176.
[97] S. Carabineiro, S. Bastos, J. Órfão, M. Pereira, J. Delgado, J. Figueiredo, Exotemplated ceria catalysts with gold for CO oxidation, Applied Catalysis A: General 381(1-2) (2010) 150-160.
[98] Z. Ferencz, A. Erdohelyi, K. Baán, A. Oszkó, L. Óvári, Z. Kónya, C. Papp, H.-P. Steinrück, J. Kiss, Effects of support and Rh additive on Co-based catalysts in the ethanol steam reforming reaction, ACS Catalysis 4(4) (2014) 1205-1218.
[99] S. Liang, F. Teng, G. Bulgan, R. Zong, Y. Zhu, Effect of phase structure of MnO2 nanorod catalyst on the activity for CO oxidation, The Journal of Physical Chemistry C 112(14) (2008) 5307-5315.
[100] X. Tang, J. Chen, X. Huang, Y. Xu, W. Shen, Pt/MnOx–CeO2 catalysts for the complete oxidation of formaldehyde at ambient temperature, Applied Catalysis B: Environmental 81(1-2) (2008) 115-121.
[101] S. Hamoudi, A. Sayari, K. Belkacemi, L. Bonneviot, F. Larachi, Catalytic wet oxidation of phenol over PtxAg1− xMnO2/CeO2 catalysts, Catalysis today 62(4) (2000) 379-388.
[102] B.-Y. Chang, C.-Y. Wang, H.-F. Lai, R.-J. Wu, M. Chavali, Evaluation of Pt/In2O3–WO3 nano powder ultra-trace level NO gas sensor, Journal of the Taiwan Institute of Chemical Engineers 45(3) (2014) 1056-1064.

[103] Y. Lv, J. Li, S. Feng, P. Liu, F. Hao, W. Xiong, H.a. Luo, Multi-walled carbon nanotubes supported nickel nanoparticles doped with magnesia and copper for adiponitrile hydrogenation with high activity and chemoselectivity under mild conditions, Chemical Engineering Journal 346 (2018) 203-216.
[104] M. Sun, J. Xia, H. Wang, X. Liu, Q. Xia, Y. Wang, An efficient NixZryO catalyst for hydrogenation of bio-derived methyl levulinate to γ-valerolactone in water under low hydrogen pressure, Applied Catalysis B: Environmental 227 (2018) 488-498.
[105] A. Reynoso, J. Ayastuy, U. Iriarte-Velasco, M. Gutiérrez-Ortiz, Cobalt aluminate spinel-derived catalysts for glycerol aqueous phase reforming, Applied Catalysis B: Environmental 239 (2018) 86-101.
[106] B. Ouyang, S. Xiong, Y. Zhang, B. Liu, J. Li, The study of morphology effect of Pt/Co3O4 catalysts for higher alcohol synthesis from CO2 hydrogenation, Applied Catalysis A: General 543 (2017) 189-195.
[107] H. Bahruji, M. Bowker, G. Hutchings, N. Dimitratos, P. Wells, E. Gibson, W. Jones, C. Brookes, D. Morgan, G. Lalev, Pd/ZnO catalysts for direct CO2 hydrogenation to methanol, Journal of Catalysis 343 (2016) 133-146.
[108] L. Lin, S. Yao, Z. Liu, F. Zhang, L. Na, D. Vovchok, A. Martinez-Arias, R. Castaneda, J.Y. Lin, S.D. Senanayake, In-situ Characterization of Cu/CeO2 Nanocatalysts during CO2 Hydrogenation: Morphological Effects of Nanostructured Ceria on the Catalytic Activity, The Journal of Physical Chemistry C (2018).
[109] Q. Liu, B. Bian, J. Fan, J. Yang, Cobalt doped Ni based ordered mesoporous catalysts for CO2 methanation with enhanced catalytic performance, International Journal of Hydrogen Energy 43(10) (2018) 4893-4901.
[110] Z. He, Q. Qian, J. Ma, Q. Meng, H. Zhou, J. Song, Z. Liu, B. Han, Water-Enhanced Synthesis of Higher Alcohols from CO2 Hydrogenation over a Pt/Co3O4 Catalyst under Milder Conditions, Angewandte Chemie International Edition 55(2) (2016) 737-741.
[111] Z. Liu, J. Zhou, K. Cao, W. Yang, H. Gao, Y. Wang, H. Li, Highly dispersed nickel loaded on mesoporous silica: One-spot synthesis strategy and high performance as catalysts for methane reforming with carbon dioxide, Applied Catalysis B: Environmental 125 (2012) 324-330.
[112] C. Yingjie, F. Yu, F. He, K. Wenbo, Y. Changkun, P. Bingrong, Z. Jun, S. Yuhan, A Nickel-Based Perovskite Catalyst with a Bimodal Size Distribution of Nickel Particles for Dry Reforming of Methane, ChemCatChem 10(9) (2018) 2078-2086.
[113] Y. Pang, Y. Dou, A. Zhong, W. Jiang, L. Gu, X. Feng, W. Ji, C.-T. Au, Nanostructured Ru-Co@ SiO2: Highly efficient yet durable for CO2 reforming of methane with a desirable H2/CO ratio, Applied Catalysis A: General 555 (2018) 27-35.
[114] R. Razzaq, C. Li, M. Usman, K. Suzuki, S. Zhang, A highly active and stable Co4N/γ-Al2O3 catalyst for CO and CO2 methanation to produce synthetic natural gas (SNG), Chemical Engineering Journal 262 (2015) 1090-1098.
[115] W. Gac, M. Greluk, G. Słowik, S. Turczyniak-Surdacka, Structural and surface changes of cobalt modified manganese oxide during activation and ethanol steam reforming reaction, Applied Surface Science 440 (2018) 1047-1062.
[116] Y.I. Choi, S.K. Kim, S.W. Lee, Y. Sohn, Metallic indium spheres by the anaerobic ethanol oxidation of indium oxide, Journal of Alloys and Compounds 687 (2016) 611-615.
[117] X. Fang, J. Zhang, J. Liu, C. Wang, Q. Huang, X. Xu, H. Peng, W. Liu, X. Wang, W. Zhou, Methane dry reforming over Ni/Mg-Al-O: On the significant promotional effects of rare earth Ce and Nd metal oxides, Journal of CO2 Utilization 25 (2018) 242-253.
[118] D. Wang, J. Guo, D. Hu, Q. Xu, L. Zhang, J. Wang, Co@ Co3O4 prepared in situ from metallic Co as an efficient semiconductor catalyst for photocatalytic water oxidation, ACS Sustainable Chemistry & Engineering (2018).